[American Journal of Science, Vol. 315, January, 2015, P. 1–45, DOI 10.2475/01.2015.01]

American Journal of Science

JANUARY 2015

STRATIGRAPHIC EXPRESSION OF EARTH'S DEEPEST $\delta^{13}C$ EXCURSION IN THE WONOKA FORMATION OF SOUTH AUSTRALIA

JON M. HUSSON*,***,†, ADAM C. MALOOF*, BLAIR SCHOENE*, CHRISTINE Y. CHEN*,**, and JOHN A. HIGGINS*

ABSTRACT. **The most negative carbon isotope excursion in Earth history is found in carbonate rocks of the Ediacaran Period (635-541 Ma). Known colloquially as the "Shuram" excursion, workers have long noted its broad concordance with the rise of abundant macro-scale fossils in the rock record, collectively known as the "Ediacaran Biota." Thus, the Shuram excursion has been interpreted by many in the context of a dramatically changing redox state of the Ediacaran oceans—for example, a result of methane cycling in a low O_2 atmosphere, the final destruction of a large pool of recalcitrant dissolved organic carbon (DOC), and the step-wise oxidation of the Ediacaran oceans. More recently, diagenetic interpretations of the Shuram excursion have challenged the various redox models, with the very negative $\delta^{13}C$ values of Ediacaran carbonates explained via sedimentary in-growth of very $\delta^{13}C$ depleted authigenic carbonates, meteoric alteration or late-stage burial diagenesis. A stratigraphic and sedimentological context is required to discriminate between these explanatory models, and to determine whether the Shuram excursion can be used to evaluate oxygenation in terminal Neoproterozoic oceans. Here we present chemostratigraphic data ($\delta^{13}C$, $\delta^{18}O$, and trace element abundances) from 15 measured sections of the Ediacaran-aged Wonoka Formation (Fm.) of South Australia. In some locations, the Wonoka Fm. is ~700 meters (m) of mixed shelf limestones and siliciclastics that record a 17 permil $\delta^{13}C$ excursion (−12 to +5‰). Further north in the basin, the Wonoka Fm. is host to deep (~1 km) paleocanyons, which are partly filled by tabular-clast carbonate breccias. Canyon-filling ceased during ongoing sedimentation on the shelf interior (the "canyon-shoulder"), as evidenced by upper canyon-shoulder units that overlie and cap certain canyon-fill sequences. The unprecedented size of the chemostratigraphic dataset presented here (2671 $\delta^{13}C$-$\delta^{18}O$ measurements from the canyon-shoulder, 1393 $\delta^{13}C$-$\delta^{18}O$ measurements from canyon clasts, and 11 different trace elements measured on 247 Wonoka Fm. carbonate samples), when coupled with the unique canyon-shoulder to canyon-fill depositional system of the Wonoka Fm., allows for new insights into Ediacaran carbon isotope systematics. The excursion is preserved in a remarkably consistent fashion across 12,000 km^2 of basin area; fabric-altering diagenesis, where present, occurs at the sub-meter vertical scale, results in < 1 permil offsets in $\delta^{13}C$ and cannot be used to explain the full $\delta^{13}C$ excursion. Multi-variate analysis of the dataset allows for rigorous assessment of different potential carbonate sources for the Wonoka canyon-fill breccias. Eroded and transported canyon-shoulder carbonates are the most likely source, thus requiring a syn-depositional age for the extraordinary range of $\delta^{13}C$ values (−12 to +5‰) observed in both the Wonoka Fm. canyon-shoulder and canyon-fill breccias. Geological**

* Department of Geosciences, Princeton University, Guyot Hall, Washington Road, Princeton, New Jersey 08544, USA

** Earth, Atmospheric and Planetary Sciences, Massachusetts Institute of Technology, 77 Massachusetts Avenue, Cambridge, Massachussetts, 02139

*** Present address: Department of Geoscience, University of Wisconsin-Madison, 1215 W. Dayton Street, Madison, Wisconsin 53706

† Corresponding author: Tel: (608) 262-8960; Fax: (608) 262-0693; E-mail: husson@wisc.edu

observations (for example, excellent preservation of sedimentary structures in Wonoka carbonates, absence of top-down alteration profiles associated with exposure surfaces) do not provide first-order evidence for the meteoric or authigenic carbonate models. Thus, the balance of evidence supports either a primary origin or syndepositional, fabric-retentive diagenesis for the deep negative $\delta^{13}C$ excursion hosted in the Wonoka Formation of South Australia.

Key words: Neoproterozoic chemostratigraphy, Shuram excursion, Wonoka paleocanyons, isotope conglomerate test

INTRODUCTION

The Ediacaran Period [635-541 Ma; Knoll and others (2006)] is host to a fundamental change to Earth's surface environment and biotic system: the rise of macroscopic animal life. While the first appearance of animal life may not rest in the Ediacaran, with sponges (Wallace and Woon, 2008; Love and others, 2009; Neuweiler and others, 2009; Maloof and others, 2010; Sperling and others, 2010; Brain and others, 2012) potentially appearing before the ~635 Ma (Hoffmann and others, 2004; Condon and others, 2005; Calver and others, 2013) terminal-Cryogenian ice age, decimeter-scale organisms [variously interpreted as animals, giant protists, macroalgae and lichen, and known as the Ediacaran Biota; Xiao and Laflamme (2009)] do not appear until ~579 Ma (Bowring and others, 2003). In broad synchroneity with these biological first appearances, marine carbonate successions on at least four continents record extreme carbon isotopic depletion; with $\delta^{13}C$ values of carbonate ($\delta^{13}C_{carb}$) dropping from +5 permil down to −12 permil, it is the deepest $\delta^{13}C_{carb}$ excursion in Earth history. This excursion is known most famously from Oman (Burns and Matter, 1993; Fike and others, 2006; Le Guerroué and others, 2006a), South Australia (Calver, 2000; Husson and others, 2012), south China (McFadden and others, 2008), and southwestern USA (Corsetti and others, 2003; Kaufman and others, 2007; Verdel and others, 2011; Bergmann and others, 2011), but also from southern Siberia (Pokrovskii and others, 2006; Melezhik and others, 2009), Scotland (Prave and others, 2009), Namibia (Saylor and others, 1998; Workman and others, 2002), northwestern Canada (Macdonald and others, 2013), northwestern Mexico (Loyd and others, 2012) and perhaps Norway (Melezhik and others, 2008). The extreme isotopic depletion seen in these Ediacaran basins is colloquially referred to as the "Shuram" excursion, named after the host formation in Oman. While at least synchronous at the period level, whether the excursions in various basins are coeval at finer temporal scales (~1 Myr) remains to be established (Grotzinger and others, 2011). Chemostratigraphic data from Scotland (Prave and others, 2009) and sparse geochronologic data (Condon and others, 2005; Bowring and others, 2007) suggest that the globally-observed excursions, synchronous or not, are hosted in sediments younger than the ~580 Ma Gaskiers glaciation [based on the appearance of a negative $\delta^{13}C_{carb}$ excursion stratigraphically above glacial strata interpreted to be Gaskiers-correlative; Prave and others (2009)] and older than a ~551 Ma ash intercalated in south China strata (Condon and others, 2005) which hosts the "Shuram" excursion.

Due to the absence of high-resolution biostratigraphy and a paucity of U-Pb ages, carbon isotope chemostratgraphy has become arguably the most important correlation tool for the Precambrian (Knoll and Walter, 1992). Chemostratigraphers rely upon a model wherein the $\delta^{13}C$ in carbonate rock reflects the $\delta^{13}C$ of dissolved inorganic carbon (DIC) in contemporaneous global sea water. The long residence time of DIC (~10^5 years), when compared to the mixing time of the oceans (~ 10^3 years), means that the $\delta^{13}C$ of DIC is nearly uniform across the globe – especially when compared to the scale of isotopic change expressed in the Ediacaran (~ 17‰). As these deep $\delta^{13}C$ excursions are globally observed phenomena, with similar shapes and

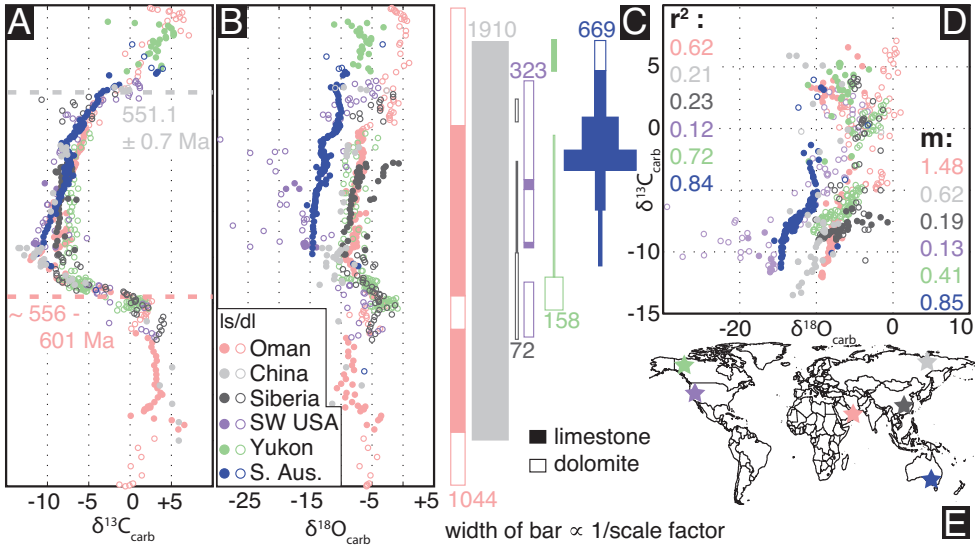

Fig. 1. "Shuram" excursion $\delta^{13}C_{carb}$ (A) and $\delta^{18}O_{carb}$ (B) data from Oman (Fike and others, 2006), south China (McFadden and others, 2008), Siberia (Pokrovskii and others, 2006), southwestern USA (Verdel and others, 2011), the Yukon (Macdonald and others, 2013), and South Australia (this work) plotted by continent and by lithology (limestone vs. dolomite). The complete recovery from the excursion has been dated in only one section [551.1 ± 0.7 Ma in south China; Condon and others (2005)], but there is almost no geochronologic control on its initiation, and duration estimates range from 5 (Bowring and others, 2007) to 50 Myr (Le Guerroué and others, 2006c). Thus, the similar $\delta^{13}C_{carb}$ profiles have been used to correlate the sections. (C) The width of the bars, color-coded by continent and lithology and labeled with true section thicknesses (in meters), correlates with 1/S, where S is the stretch factor applied to each dataset. If the Shuram excursion is an expression of secular change in global DIC, then the width of the bars would also correlate with relative sedimentation rates of each section. (D) It is widely assumed that all Shuram excursion datasets display strong covariation between $\delta^{13}C_{carb}$ and $\delta^{18}O_{carb}$, especially for samples with $\delta^{13}C_{carb} < -5‰$. A cross-plot of this compiled Ediacaran dataset, however, with correlation coefficients between $\delta^{13}C_{carb}$ and $\delta^{18}O_{carb}$ listed by section [for $\delta^{13}C_{carb}$ values $< -5‰$; p values $<<0.001$ except for Siberia ($p = 0.01$) and southwestern USA ($p = 0.025$)], shows that the correlation ranges from strong ($r^2 = 0.84$ in South Australia) to weak ($r^2 = 0.12$ in southwestern USA) with linear slopes ranging from 1.5 to 0.1. (E) World map showing present-day location of all sections used in this compilation.

magnitudes, and hosted in basins of broadly Ediacaran age, it has been argued that the "Shuram" excursion fits the model of a global carbon cycle perturbation and can therefore can be used as a global stratigraphic tie-point (figs. 1 and 2A).

If the Shuram excursion is a primary signal, its extreme nature, with observed $\delta^{13}C_{carb}$ well below the canonical value of ~ −6 permil for mantle carbon input to the ocean-atmosphere system, requires a distinctly non-uniformitarian Ediacaran carbon cycle. Current primary DIC models focus on sustained fluxes of re-mineralized organic carbon, in the form of either methane hydrates (Bjerrum and Canfield, 2011) or a large pool of recalcitrant particulate and dissolved organic carbon [the "big DOC" model; Rothman and others (2003)], to the hydrosphere, made possible by lower O_2 concentrations in the Ediacaran (Canfield and others, 2007; Scott and others, 2008; Johnston and others, 2012). One challenge in assessing these models is that absolute time constraints are necessary to quantify the light carbon fluxes and oxidant budget required to drive the excursion, both of which would be unrealistically large if the excursion lasted much longer than ~1 million years (Myr) (Bristow and Kennedy, 2008). Although a U-Pb zircon tuff date of 551.1 ± 0.7 Ma from the Doushantuo Formation provides a minimum age constraint on the complete recovery from the Shuram excursion (Condon and others, 2005), the best maximum age constraint is a

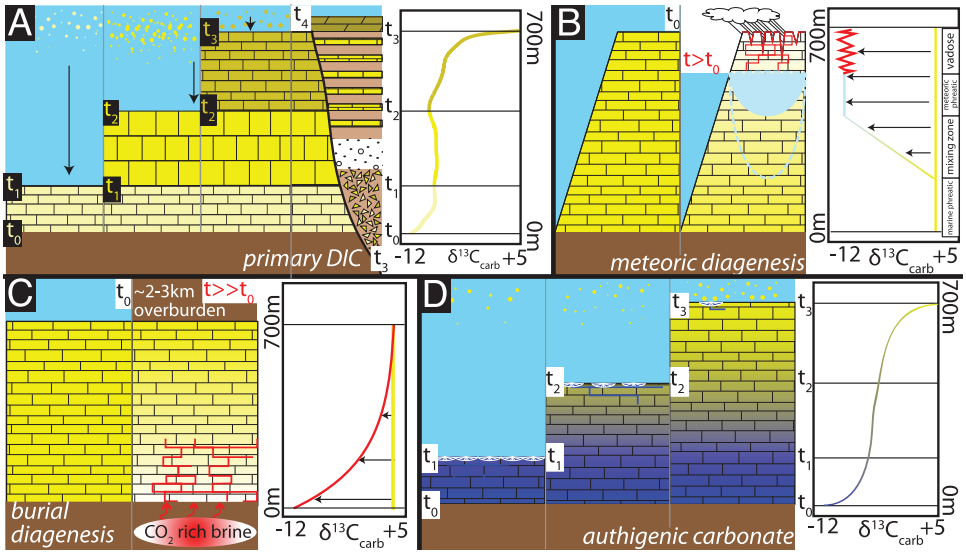

Fig. 2. Schematic cartoons illustrating the four main hypotheses which seek to explain the "Shuram" excursion in South Australia. (A) Primary DIC models contend that the excursion is a result of a secular change in the isotopic composition of DIC; thus the excursion is "built" as the carbonate succession is assembled (from t_0 to t_3). In the case of South Australia, recovery from the excursion also coincides with substantial erosion and mass wasting of the carbonate succession. Meter-thick breccias of canyon cut-fill sequences (t_3 to t_4) consist of clasts of eroded canyon-shoulder carbonates and host the same $\delta^{13}C_{carb}$ variability (−12 to +5‰) as the intact canyon-shoulder profile (Husson and others, 2012). (B) Under the meteoric model, a carbonate succession with "normal" isotopic values (t_0) is subaerially exposed ($t > t_0$), and depleted $\delta^{13}C_{carb}$ values are the result of overprinting by recrystallizing fluids charged with DIC issued from organic matter respiration in soils (Knauth and Kennedy, 2009; Swart and Kennedy, 2012). A first order-prediction of this model is that the most negative $\delta^{13}C_{carb}$ values in an isotopic profile should be associated with exposure surfaces. Black arrows indicate the direction of diagenetic alteration imposed by the topdown invading fluid. (C) The burial diagenesis model invokes post-burial fluid-rock interactions at depth, wherein a high pCO_2, low $\delta^{13}C$ fluid, developed from buried organic matter, mixes with an ^{18}O-rich basinal brine (Derry, 2010). Black arrows indicate the direction of diagenetic alteration of the original isotopic profile (values at t_0) imposed by bottom-up fluid flow, altered towards lighter values at $t >> t_0$. (D) The authigenic carbonate model seeks to explain negative $\delta^{13}C_{carb}$ excursions as a result of sedimentary in-growth of very $\delta^{13}C$ depleted carbonates during early sediment diagenesis, wherein authigenic carbonates constitute the largest mass fraction in horizons with the most negative $\delta^{13}C_{carb}$ values.

SHRIMP UPb detrital zircon population age of 609 ± 7 Ma from the Khufai Formation in Oman (Le Guerroué and others, 2006c). Therefore, the duration of the Shuram excursion is poorly constrained, with estimates ranging from 5 (Bowring and others, 2007) to 50 Myr (Le Guerroué and others, 2006c).

In recent years, focus has shifted from further developing DIC models for the Shuram excursion towards questioning the primary nature of Ediacaran $\delta^{13}C_{carb}$ records. This shift has profound implications both for our understanding of Ediacaran redox evolution and the rise of metazoans [for example, Fike and others (2006); McFadden and others (2008)], and for the utility of Shuram-like profiles in Ediacaran successions as an inter-basin correlation tool [for example, Halverson and others (2005)]. The alternative hypotheses are diagenetic in nature, and include (1) meteoric diagenesis, (2) burial diagenesis and (3) authigenic carbonate models. Under the meteoric model, the negative $\delta^{13}C_{carb}$ values and covarying $\delta^{13}C_{carb}$-$\delta^{18}O_{carb}$ [features of most, but not all (Verdel and others, 2011; Lee and others, 2013), Shuram-like excursion profiles; fig. 1D] are interpreted as a result of recrystallization in the presence of CO_2-rich fluids, derived from organic matter re-mineralization in soils [Knauth and Kennedy (2009); Swart and Kennedy (2012); fig. 2B]. Sourced from ^{18}O-depleted

rainwater, these fluids can create covarying $\delta^{13}C_{carb}$-$\delta^{18}O_{carb}$ arrays as they mix with marine waters heavier in both $\delta^{13}C_{carb}$ and $\delta^{18}O_{carb}$ (Allan and Matthews, 1982). This process exerts significant control over $\delta^{13}C_{carb}$ values in late Cenozoic carbonates from the Great Bahama Bank (Melim and others, 2001; Swart and Eberli, 2005; Swart, 2008; Swart and Kennedy, 2012), where negative shifts in $\delta^{13}C_{carb}$ are driven by ice-age related sea level falls and consequent infiltration of coastal pore fluids. These profiles also are characterized by pervasive, fabric-destructive recrystallization (Melim and others, 2001), which is not observed in successions that host the Shuram excursion (Le Guerroué and others, 2006a; McFadden and others, 2008; Melezhik and others, 2009; Husson and others, 2012). Additionally, there is no widely accepted, independent evidence for the presence of a significant terrestrial biomass in the Ediacaran to act as a source for depleted carbon.[1]

The burial diagenesis model contends that extreme depletion in $\delta^{13}C_{carb}$ was acquired significantly after burial of Ediacaran sediments [for example, under 2–3 km of overburden, at ~100 °C; Derry (2010)]. "Shuram" excursion profiles result from alteration by a mixture between a high pCO_2, low $\delta^{13}C_{carb}$ fluid, developed from respired buried organic matter, and an ^{18}O-rich basinal brine (Derry (2010); fig. 2C). Geochemical models simulating this scenario have been able to reproduce the covarying $\delta^{13}C_{carb}$-$\delta^{18}O_{carb}$ arrays common to Ediacaran successions (fig. 1D). Isotope conglomerate tests from the Ediacaran-aged Wonoka Formation (Fm.) of South Australia, however, require a syn-depositional age for the extraordinary range of $\delta^{13}C_{carb}$ values (−12 to +5‰) observed in the formation (Husson and others, 2012). In some locations, the Wonoka Fm. is ~700 meters (m) of mixed shelf limestones and siliciclastics; further outboard, the Wonoka Fm. is host to deep (~1 km) paleocanyons, which are partly filled by tabular-clast carbonate breccias that are sourced from eroded Wonoka canyon-shoulders. Canyon formation occurred during ongoing Wonoka sedimentation, and they were filled before deposition of the upper-most ~100 m of Wonoka canyon-shoulder had occurred (Husson and others, 2012). Canyon-shoulder sections host the full 17 permil $\delta^{13}C_{carb}$ excursion (fig. 1A), as well as co-variation between $\delta^{13}C_{carb}$ and $\delta^{18}O_{carb}$ (fig. 1D); likewise, the redeposited clasts exhibit the same extremely depleted $\delta^{13}C_{carb}$ values and strong correlation between $\delta^{13}C_{carb}$ and $\delta^{18}O_{carb}$. These observations require that both the negative $\delta^{13}C_{carb}$ values and the $\delta^{13}C_{carb}$-$\delta^{18}O_{carb}$ covariation were acquired in Wonoka Fm. canyon-shoulder carbonates before those carbonates were brecciated and re-deposited in the paleocanyons, and could not have been developed as a result of late-stage burial diagenesis (Husson and others, 2012).

The authigenic carbonate model calls upon the sedimentary in-growth of very $\delta^{13}C$ depleted carbonates during early sediment diagenesis to explain the development of Shuram-like $\delta^{13}C_{carb}$ profiles [Schrag and others (2013); fig. 2D]. In the modern ocean, most authigenic carbonate is formed when alkalinity is produced from anoxic respiration of organic carbon and accompanying reduction of sulfate and ferric iron, which results in the over-saturation of $CaCO_3$ in pore fluids. Such processes were perhaps more important in the Neoproterozoic, with putatively lower O_2 concentrations allowing for widespread bottom-water $CaCO_3$ over-saturation, thus making seafloor $CaCO_3$ cements and precipitates more significant alkalinity sinks than they are in the more oxic Phanerozoic (Higgins and others, 2009). From a geological perspective, these seafloor carbonates have distinctive textures, appearing in the rock record as crystal fans, void-filling cements, and secondary nodules (Grotzinger and James, 2000). First-order geological evidence that supports the authigenic model, therefore,

[1] While a new interpretation of South Australian Ediacaran Biota as preserved lichens recently has been proposed (Retallack, 2013), this view is controversial (Xiao and others, 2013).

would be documentation of such fabrics in Ediacaran successions that host Shuram-like excursions (Pruss and others, 2008; Macdonald and others, 2013). More generally, all three diagenetic models argue for acquisition of negative $\delta^{13}C_{carb}$ values after Ediacaran carbonate sediments had been deposited (although in the meteoric and authigenic models, alteration can happen immediately after deposition), thereby severing the connection between $\delta^{13}C_{carb}$ and the $\delta^{13}C$ of Ediacaran DIC. If the "Shuram" excursions are a record of alteration, one must ask (a) why sediment diagenesis, fundamentally a local process, would lead to global isotopic resetting of Ediacaran carbonate basins (synchronously or not) and (b) why might this process of "global diagenesis" be restricted in time to the Ediacaran Period (Grotzinger and others, 2011; Schrag and others, 2013).

Whereas basin-scale physical- and chemo-stratigraphic studies of the Shuram excursion have been undertaken in Oman (Le Guerroué and others, 2006a, 2006b) and the southwest US (Verdel and others, 2011; Bergmann and others, 2011), no such survey exists for South Australia, with most studies of the Ediacaran "Shuram" excursion focusing on single sections and global correlations. Here we present 3075 $\delta^{13}C_{carb}$-$\delta^{18}O_{carb}$ measurements from fifteen 500 to 1500-m-thick stratigraphic sections (figs. 3, 4 and 5), 1393 $\delta^{13}C_{carb}$-$\delta^{18}O_{carb}$ measurements from canyon-fill clasts, and 247 trace element abundance measurements from the Ediacaran Wonoka Fm. of the Adelaide Rift Complex (ARC) of South Australia. All data are available online as a supplementary electronic data file (http://earth.geology.yale.edu/~ajs/SupplementaryData/2015/02HussonDATA.xlsx). Of this dataset, $\delta^{13}C_{carb}$-$\delta^{18}O_{carb}$ measurements from measured sections 6–8 and 13–15 (n = 1049) and on 485 clasts were previously published in Husson and others (2012). The full dataset (a) shows the remarkable consistency of a Shuram-like $\delta^{13}C_{carb}$ excursion (down to −12‰) across ~12,000 square kilometers of basin area, (b) constrains the relative timing of Wonoka canyon incisions, (c) documents that fabric-destructive diagenesis, where present, occurs at the sub-meter vertical scale, results in < 1 permil offsets in $\delta^{13}C_{carb}$ and cannot be used to explain the full $\delta^{13}C_{carb}$ excursion, (d) corroborates and expands upon the isotope conglomerate tests of Husson and others (2012) and their exclusion of late-stage diagenesis and (e) constrains the styles of early-stage diagenesis that could be invoked to explain the $\delta^{13}C_{carb}$ excursion from South Australia that are consistent with geological observations.

GENERAL BACKGROUND

Adelaide Rift Complex

The Adelaide Rift Complex (ARC; fig. 3) was part of a continental margin formed to the present day east of the Stuart Shelf (Preiss, 2000). Although clearly overlapping in time, correlation between the ARC and thinner cratonic basins in central and northern Australia is difficult because the ARC was a zone of deep subsidence, punctuated by episodes of syn-sedimentary faulting and diapiric mobilization of Callanna Group evaporites. The ARC contains very thick Neoproterozoic and Cambrian sequences that were folded during the Cambro-Ordivician Delamerian orogeny (Thomson and others, 1964) and currently are well exposed in the Flinders and Gammon ranges (Preiss, 1987). The basal clastics of the Burra Group (Rhynie Sandstone) overlie the Boucat volcanics, a bimodal suite of amygdaloidal basalt and rhyolitic ignimbrite with a U-Pb SHRIMP zircon age of 777 ± 7Ma [fig. 3B; Preiss (2000)]. The Callanna-Burra contact is thought to correlate to the end of the Bitter Springs negative carbon isotope Stage [fig. 3B; Hill and Walter (2000); Halverson and others (2005); Maloof and others (2006); Halverson and others (2007); Swanson-Hysell and others (2012)]. Overlying the Burra Group is the Umberatana Group, which begins with the older of two Cryogenian glacial deposits known as the Sturtian,

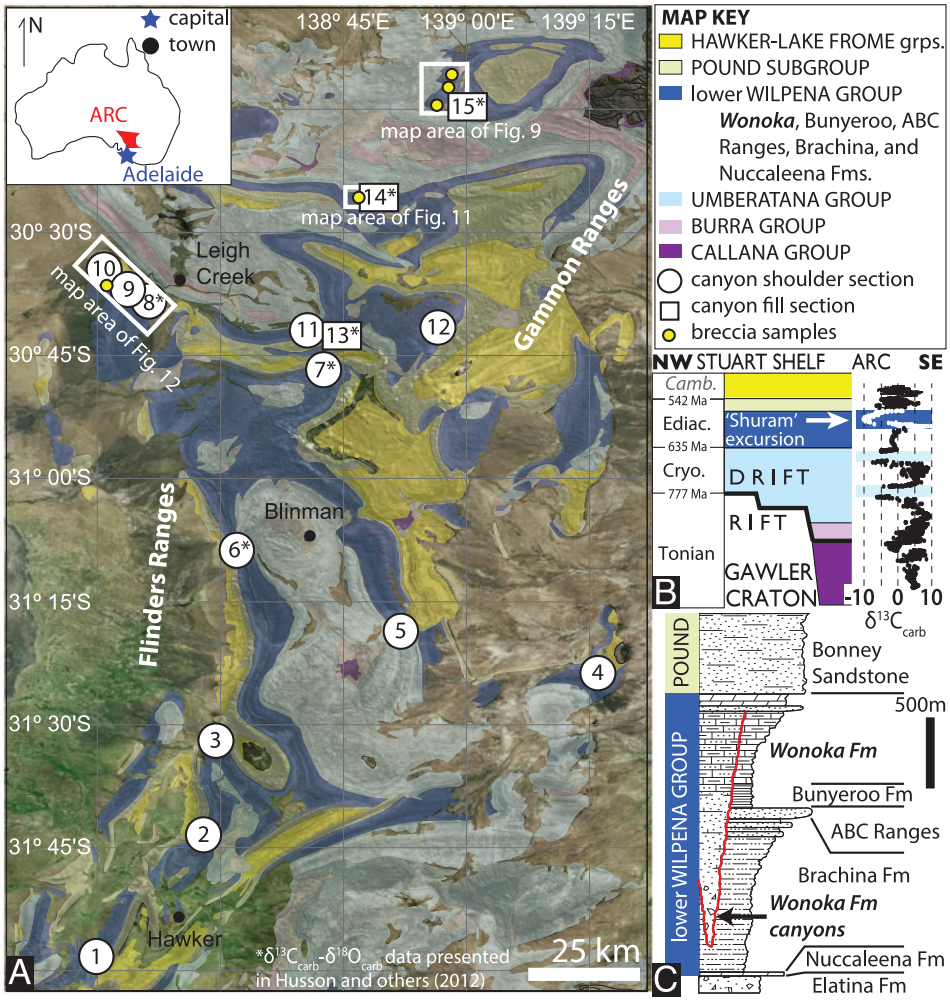

Fig. 3. (A) Simplified geological map, adapted from Raymond and others (2012) and using the WGS84 datum, of the study area within the Adelaide Rift Complex (ARC) overlying a *Bing Maps* aerial photograph. Locations of measured stratigraphic sections are denoted by white symbols, and insets for paleocanyon maps of Mount Thomas (fig. 9), Oodnapanicken (fig. 11) and Saint Ronan (fig. 12) are labeled with white outlines. (B) Schematic NW-SE stratigraphic cross section of the Adelaide Rift Complex, adapted from Rose and Maloof (2010), highlighting the rift-to-drift transition and major sequence boundaries. Composite $\delta^{13}C_{carb}$ data from Halverson and others (2005) is time-aligned with the right-hand edge of the stratigraphic cross-section. The interval highlighted in white marks the focus of this contribution. (C) Schematic physical stratigraphy, adapted from Giddings and others (2010), of the lower Wilpena Group, showing the incision of ~1000 m deep paleocanyons, emanating from the upper Wonoka Fm. (Husson and others, 2012)

and continues with a thick package of mixed siliciclastics and carbonates of the Tapley Hill, Etina, Enorama, and Trezona Formations. At the top of the Umberatana Gp. is the Elatina Formation, which is the younger of the two Cryogenian glacial deposits (Marinoan) and has an erosional unconformity with local relief of up to at least 130 m, and possibly as much as 500 m (Rose and others, 2013).

The Nuccaleena Formation, the distinctive cap dolostone to the glacial Elatina Fm (Williams, 1979; Plummer, 1979; Rose and Maloof, 2010), forms the base of the Wilpena Group (fig. 3C), and frequently is correlated to the younger Cryogenian

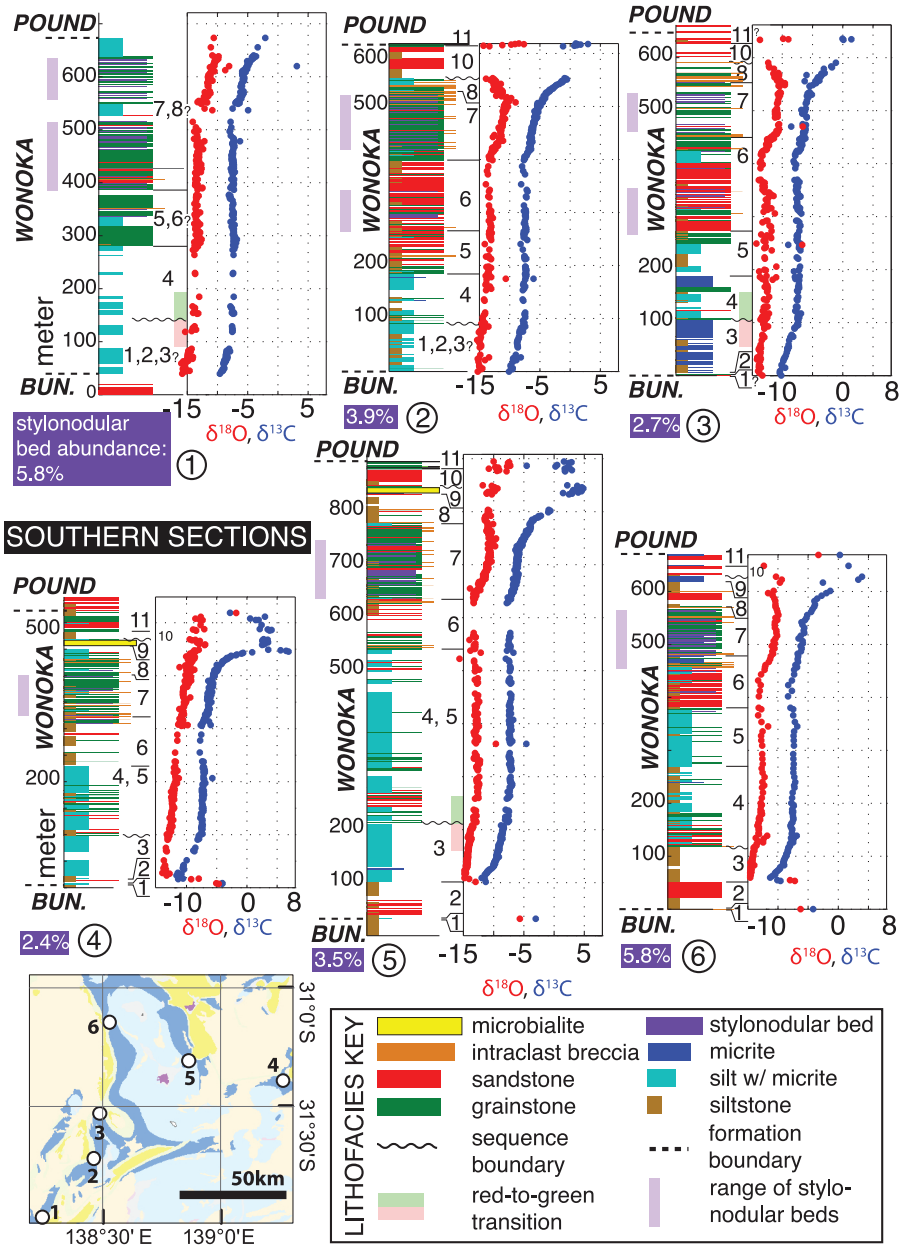

Fig. 4. Canyon-shoulder physical stratigraphy paired with $\delta^{13}C_{carb}$ and $\delta^{18}O_{carb}$ data from 6 southern localities (sections 1-6). In a given row, sections move progressively north from left to right, and are vertically aligned using the nadir of $\delta^{13}C_{carb}$ as a datum. Haines (1988) subdivided the Wonoka Formation into 11 informal lithological units, which are broadly recognizable throughout the central Flinders Ranges and labeled here on our canyon-shoulder sections. Section locations are on figure 3A and on the small inset map in the bottom-left of this figure.

glacial cap units found around the world (Halverson and others, 2005), dated to be ~635 Ma in Namibia (Hoffmann and others, 2004), south China (Condon and others, 2005), and Tasmania (Calver and others, 2013). The Nuccaleena Formation marks the

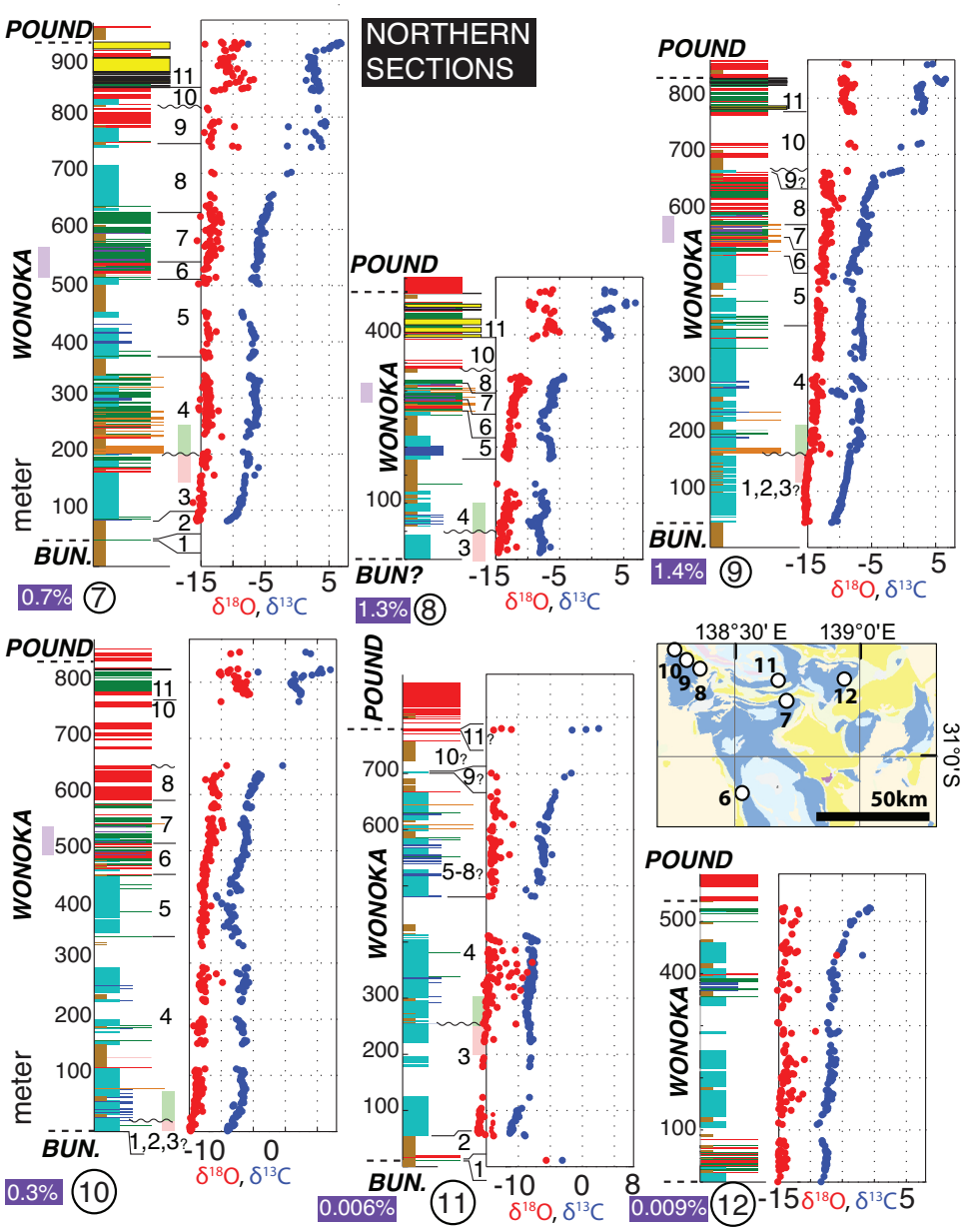

Fig. 5. Canyon-shoulder physical stratigraphy paired with $\delta^{13}C_{carb}$ and $\delta^{18}O_{carb}$ data from 6 northern localities (sections 7-12). In a given row, sections move progressively north from left to right, and are vertically aligned using the nadir of $\delta^{13}C_{carb}$ as a datum. Figure symbologies are the same as in figure 4. Section locations are on figure 3A and on the small inset map in the middle-right of this figure.

onset of the post-glacial transgression (Williams, 1977; Plummer, 1979; Dyson, 1992a; Kennedy, 1996; Rose and Maloof, 2010), which culminates in a maximum flooding surface at the base of the red and green siltstones of the overlying Brachina Fm, and eventually shallows up into the ABC Ranges shallow-marine quartzites in the central

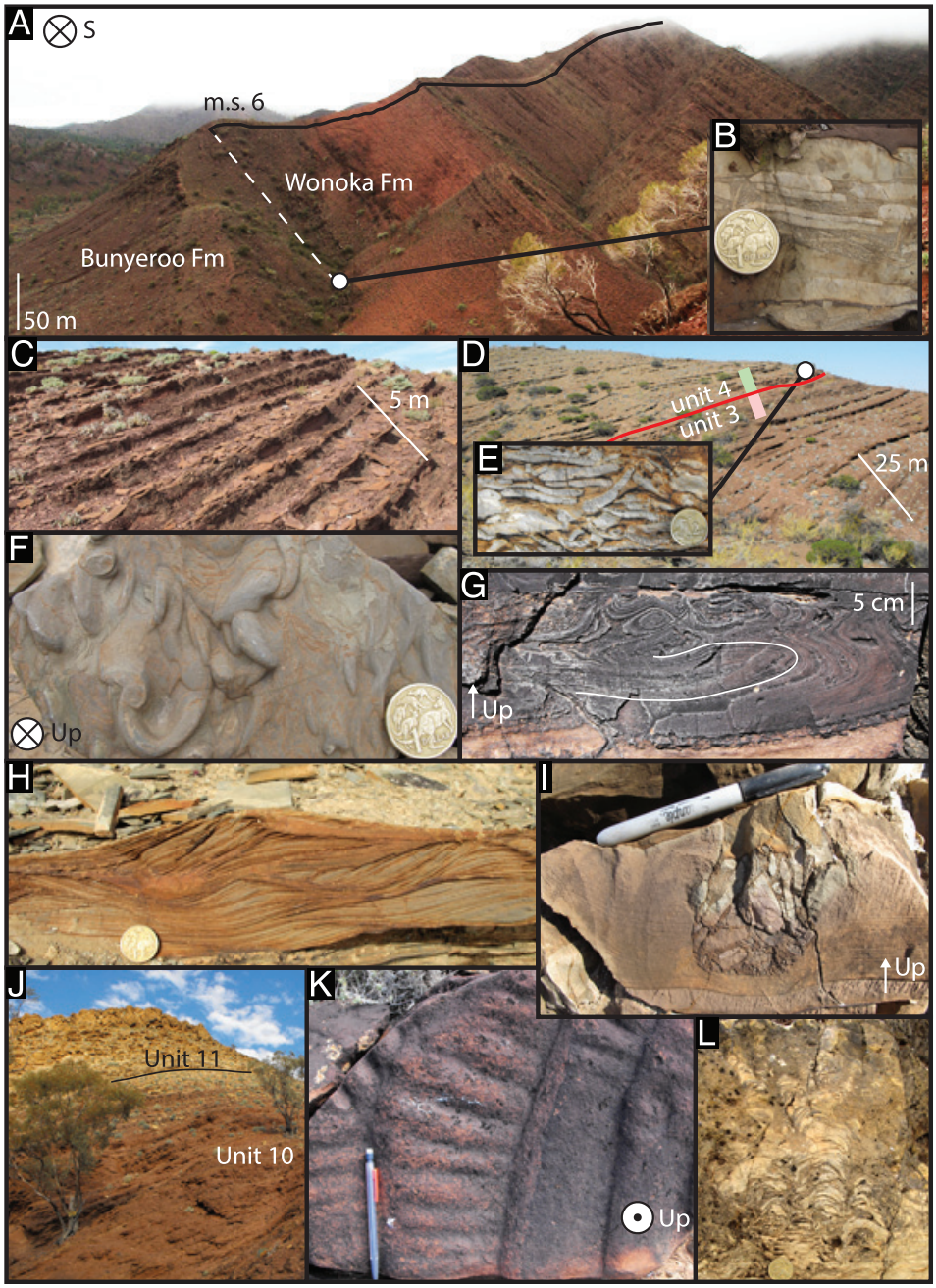

Fig. 6. Representative field photographs from Wonoka canyon-shouder sections. (A) Outcrop scale photograph of the lower ~200m of section 6, labeled with a trace of the measuring transect (fig. 4). (B) The thin (0.1-1 m), but persistent, "Wearing Dolomite" marks the base of most sections, and is often a grainstone or intra-clast tabular breccia. (C) Unit 3 is the first carbonate abundant unit in the Wonoka, and consists of thin (2-5 cm) event beds of limestone intercalated with red siltstone. Unit 3 is organized into 1–2 m packages, which coarsen and become more carbonate-rich upwards. Unit 3 ends abruptly with a sharp transition (D) from red-to-green siltstone. (E) This transition is commonly marked by a intraformational, tabular-clast limestone breccia or a 30-cm-thick green grainstone. (F) The bottoms of the lower Wonoka event beds are often fluted. The Wonoka coarsens upwards, transitioning to thicker-bedded carbonate grainstones and

Flinders Ranges. The ABC Ranges quartzite, not present in the northern part of the ARC, is overlain by a flooding surface and the purple siltstones of the Bunyeroo Formation, which contains the Acraman ejecta horizon ~80 m above its base (Gostin and others, 1986). The Wonoka Formation overlies the Bunyeroo Fm, and in places, fills deep incisions that penetrate up to 1000 meters into the underlying Bunyeroo and Brachina fms. (fig. 3C).

Physical Sratigraphy of the Wonoka Formation

The Wonoka Formation varies between 500 and 1500 meters (m) thick, and coarsens and shallows upward into the siliclastic, Ediacara Biota-bearing Pound Subgroup (fig. 3C). Haines (1990) subdivided the Wonoka Fm. into 11 informal lithological units, which are broadly recognizable throughout the central Flinders Ranges and labeled, where apparent, on the sections presented in figures 4 and 5. At its base in the central Flinders Ranges, the Wonoka Fm. is marked by the ~10 centimeter (cm) thick Wearing Dolomite, most commonly a grainstone but locally an intraclast breccia (figs. 6A and 6B). Dolomite only occurs in the Wonoka as this thin, basal marker bed and in its upper 100 to 150 meters. The Wonoka begins as a deep-shelf sequence of red siltstones intebedded with thin-bedded (2-5 cm), often fluted turbiditic carbonate beds (fig. 6C). At many localities (measured sections 1, 3, 4, and 5 on fig. 4 and 7-11 on fig. 5), the lowermost 100 to 150 m Wonoka is capped by an abrupt transition from red to green silt interbeds [fig. 6D; the unit 3-4 boundary of Haines (1990)]. This surface is sharp, and commonly marked by an intraformational, tabular-clast limestone breccia (measured sections 7, 9 on fig. 5; fig. 6E) or a thick-bedded (~30-40 cm) green grainstone. The carbonate turbidites often are fluted on their bases (fig. 6F) and develop climbing ripples near their tops. The Wonoka Fm. transitions upward into a shallower, storm-dominated midshelf sequence, containing thicker-bedded (~0.5-1 m) wavy limestone laminites and grainstones and interbedded fine sandstones, abundant evidence for slumping, ball-and-pillow structures, and soft-sediment deformation (fig. 6G), hummocky and swaley cross-stratification (fig. 6H), and pothole casts (fig. 6I).

At the top of these units, the first unequivocally shallow-water carbonates appear. Unit 9 of Haines (1990) is 5 to 40 m of black, wavy laminated microbialite; it is not present in the most southerly sections (measured sections 1-3 on fig. 4), and is thickest and mostly composed of sandy calcarenite at measured section 7 (fig. 5). Above these beds, the Wonoka Fm. transitions abruptly into a thick (~30-150 m) package of siliciclastics, in which carbonate interbeds are entirely lacking (unit 10; fig. 6J). This sequence is best developed in measured sections 8–10 (figs. 3A and 5). In this belt, the last sandy carbonate bed of unit 8/9 is flooded by silt, which coarsens progressively upwards to hummocky cross-stratified, fine sandstone and eventually to medium-coarse, sub-rounded sandstone with wave and ladder ripples (fig. 6K). The uppermost Wonoka Fm. is characterized by a return to carbonate facies, with ~5 to 100 m of dolomitized microbialite, oolitic grainstones and stromatolite bioherms (unit 11; fig. 6L). In an outcrop pattern similar to unit 9, unit 11 is not present in the most southerly section (measured section 1 on fig. 4), and thickens and deepens northward, becom-

Fig. 6 (continued) sandstones, which show abundant evidence of soft-sediment deformation (G, with thin white line tracing the fold limb), small-scale hummocky cross-stratification (H) and pothole casts (I). Above these grainstone-sandstone sequences, the Wonoka abruptly transitions to a thick (~30-150 m) package of red siliciclastics in which carbonate interbeds are entirely lacking (unit 10; J). This sequence is silty and fine at the base, and shallows to medium-coarse, sub-rounded sandstones with wave and ladder ripples (K). The uppermost Wonoka Fm. is characterized by a return to carbonate facies, with ~5–100 m of predominately yellow, dolomitized microbialite and stromatolite bioherms (unit 11; L).

ing dominated by dolomitized grainstones with stromatolite-flake breccias (measured sections 8-10 on fig. 5).

In 50 to 200 meters of thick-bedded carbonate grainstones below the unit 10 siliciclastics, primary sedimentary structures often are obscured or fully destroyed by stylonodular texture [Haines (1988); Flügel (2004), p. 318]. Stylonodular texture is a secondary fabric, wherein carbonate rock is partitioned into centimeter-to-millimeter diameter ovoid lenses by horizontally anastamozing stylolitic sheets, composed of SiO_2 or silicified limestone (figs. 7A and 7E). Alternations between stylonodular and well-laminated, primary textures can occur at the cm-scale (fig. 7B). The texture emanates from the tops of grainstone beds, often smoothly transitioning downwards from fully stylonodular to well-laminated, with nodule size increasing upwards from the bed-base (fig. 7C). Though knife sharp contacts between well-preserved textures and fully stylonodular beds are common (fig. 7D), no instance of upwardly decreasing nodule size (that is, a smooth transition upwards from fully stylonodular → partially stylonodular → no nodules) has ever been observed, thereby strengthening the notion that this phenomenon is a top-down diffusive process, originating at bed-tops. The percentage of nodular beds (measured as [total thickness of nodular beds]/[full Wonoka section thickness] × 100) decreases from south to north (figs. 4 and 5). Noting pendants and overhangs of nodular beds caused by erosion from overlying grainstones, Haines (1988) concluded that nodular formation was initiated during early lithification, prior to bed erosion by subsequent event beds.

In contrast to the shallower, storm-dominated mid-shelf sequence, the northern Flinders (11-15 in fig. 3A) record deeper outermost-shelf and slope settings. The Wonoka Fm. is finer-grained, with less sand and carbonate grainstones and more silt with interbeds of thin-bedded (2-7 cm) micrite (measured sections 11 and 12 in figs. 3A and 5). Microbialitic unit 11 is not present in these sections. Further north, ~1000-m-deep paleocanyons cut into the underlying Bunyeroo and Brachina fms. [Oodnapanicken (measured section 14) and Mount Thomas (measured section 15) on fig. 3A; see also figs. 8A, 9, 10, and 11; von der Borch and others (1989); Christie-Blick and others (1990); DiBona and von der Borch (1993); Giddings and others (2010)]. The most striking features of canyon-fill stratigraphy are the tabular-clast limestone and siltstone breccias (figs. 8B-8D), which are most common near the base of the paleocanyons (figs. 9, 11 and 12). In between breccia flows, the canyon-fill consists of meter-scale fining-upward packages of carbonate-cemented sandstone and marly siltstones. The base of these turbiditic sequences very often is fluted (fig. 8E) and the coarser-grained beds have ubiquitous climbing ripples (fig. 8F). Above these basal fill sequences, the Wonoka Fm. fines upward into couplets of siltstone and thin (2-5 cm) beds of micritic limestone. In addition to these deep canyons, shallower canyon cut-fill sequences also exist [Saint Ronan canyon, bracketed by sections 10 and 9 on figs. 3A and 12, and Mount Goddard canyon (section 13 on fig. 3A)]. At Mount Goddard, the incision cuts at least 100 to 150 m into the Bunyeroo Fm., and the canyon-fill sequence is composed entirely of grainstones and sandstones (that is, carbonate breccias are absent). At Saint Ronan, canyon-cutting has excised at least ~150 m of lower Wonoka carbonates (that is, wavy micrite interbedded with red silt; units 1, 2 and 3 on figs. 4 and 5). The canyon erosional surface is capped by thinner (sub-meter scale) breccias interbedded with green siltstone and sits on the Bunyeroo Fm. The canyon-fill sequence at Saint Ronan is blanketed by unit 11 microbialites (fig. 12A), thus indicating that the canyon at Saint Ronan had filled with re-deposited canyon-shoulder clasts *before* sedimentation on the canyon-shoulders had completed. In other words, canyon-formation was syn-depostional with Wonoka canyon-shoulder sedimentation, with unit 11 microbialites eventually prograding over canyon-fill sec-

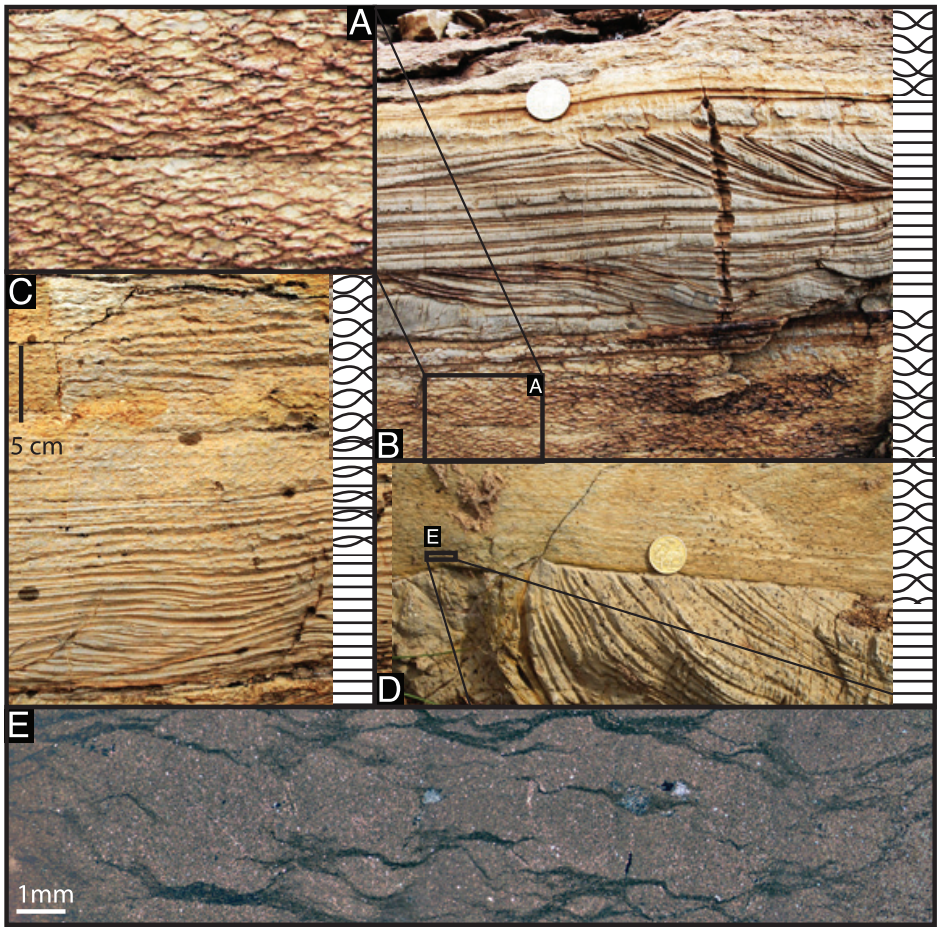

Fig. 7. Field photographs of stylonodular texture, with cartoons depicting nodule size. (A) Nodular bedding is a secondary fabric, wherein the carbonate rock is partitioned into centimeter-tomillimeter ovoid lenses by horizontally anastamosing stylolitic sheets. Nodule size often increases stratigraphically upwards over 5–10 cm of vertical distance. (B) Alternation between well preserved, cross-stratified grainstones and nodular bedding can occur at the cm scale. (C) Though often sharp, boundaries between grainstones and nodular beds can be gradual and diffuse, with a smooth transition upward from no nodules→partially stylonodular→fully stylonodular occuring over 5–10 cm thick vertical boundaries. This field photograph shows the disappearance of primary bedding textures, present at the base of the bed, as it is destroyed by nodular formation. (D) Sharp, erosive contact between a fully stylonodular bed and a well-preserved, slumped grainstone. This relationship implies that nodule formation completely over-printed the upper bed, yet failed to penetrate into the lower bed. (E) Thin section of a stylonodular bed under cross-polar light. The nodules are outlined by the darker, more silica-rich anastomosing bands.

tions. Henceforth, outer shelf sections are referred to as "canyon-shoulders", and sections with paleocanyons as "canyon-fill."

METHODS

$\delta^{13}C_{carb}$ *and* $\delta^{18}O_{carb}$ *Methods*

For canyon-shoulder and canyon-fill stratigraphic sections, carbonates were sampled at 1 to 2 m resolution (figs. 4 and 5). Mineralogy (limestone vs. dolomite) was determined in the field via the acid test, and clean carbonates with minimal siliciclastic

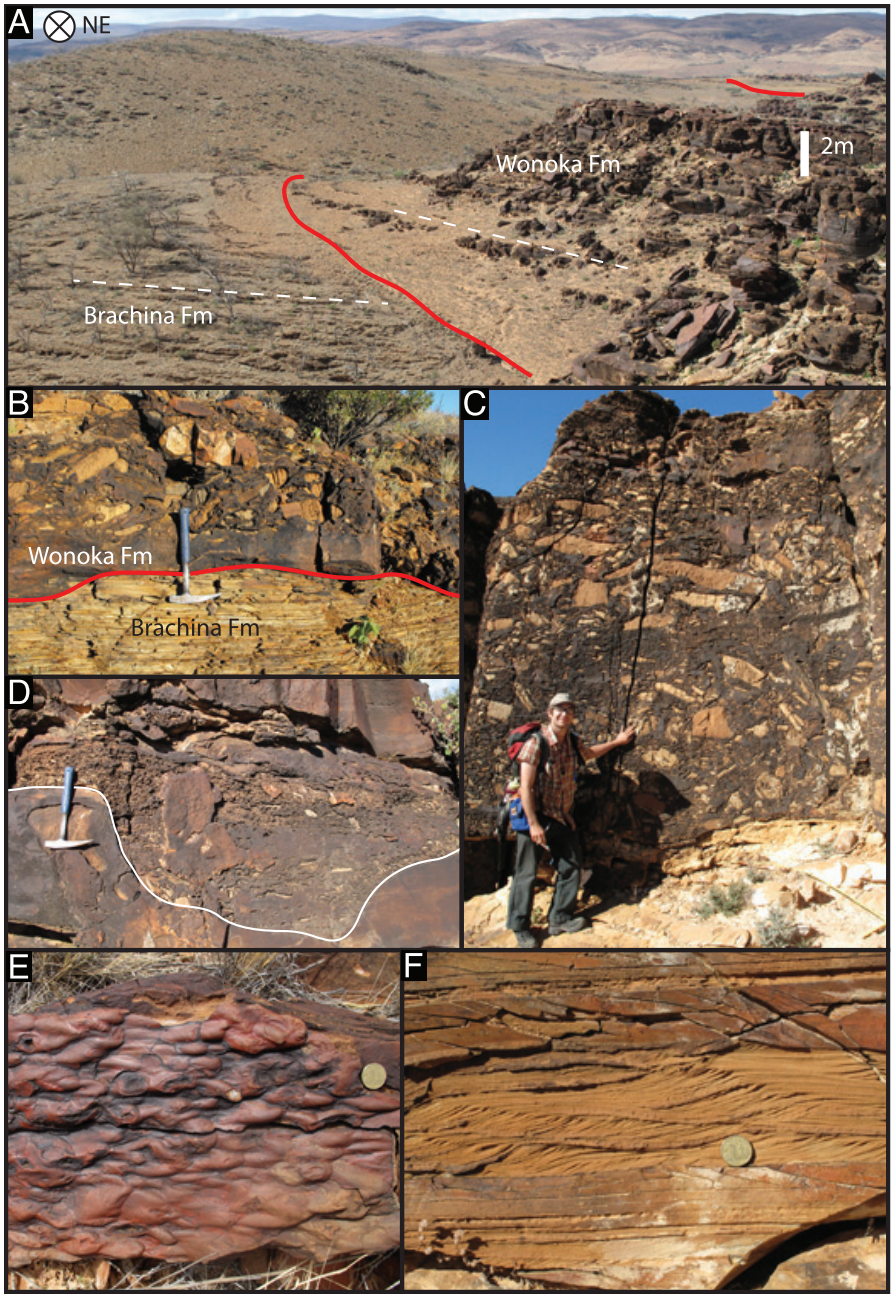

Fig. 8. Representative field photographs from Wonoka canyon-fill sections. (A) Red line marks the angular and erosive contact between the Brachina Fm. canyon wall and Wonoka Fm. canyon-fill (white dashed lines depict change in bedding attitude) at Mount Thomas (fig. 9). (B) This basal contact is most often marked by tabular-clast carbonate breccias, which can be meters thick (C) and are dominated by clasts (1-100 cm long) of micritic limestone and dolomite. (D) Within the canyon-fill stratigraphy, breccia unit contacts (white line) often have a 0.5–1 m of local relief. In between breccia units, the canyon-fill stratigraphy is dominated by fluted, fine, carbonate-cemented sandstones (E) with abundant, 2–3 cm scale climbing ripples (F).

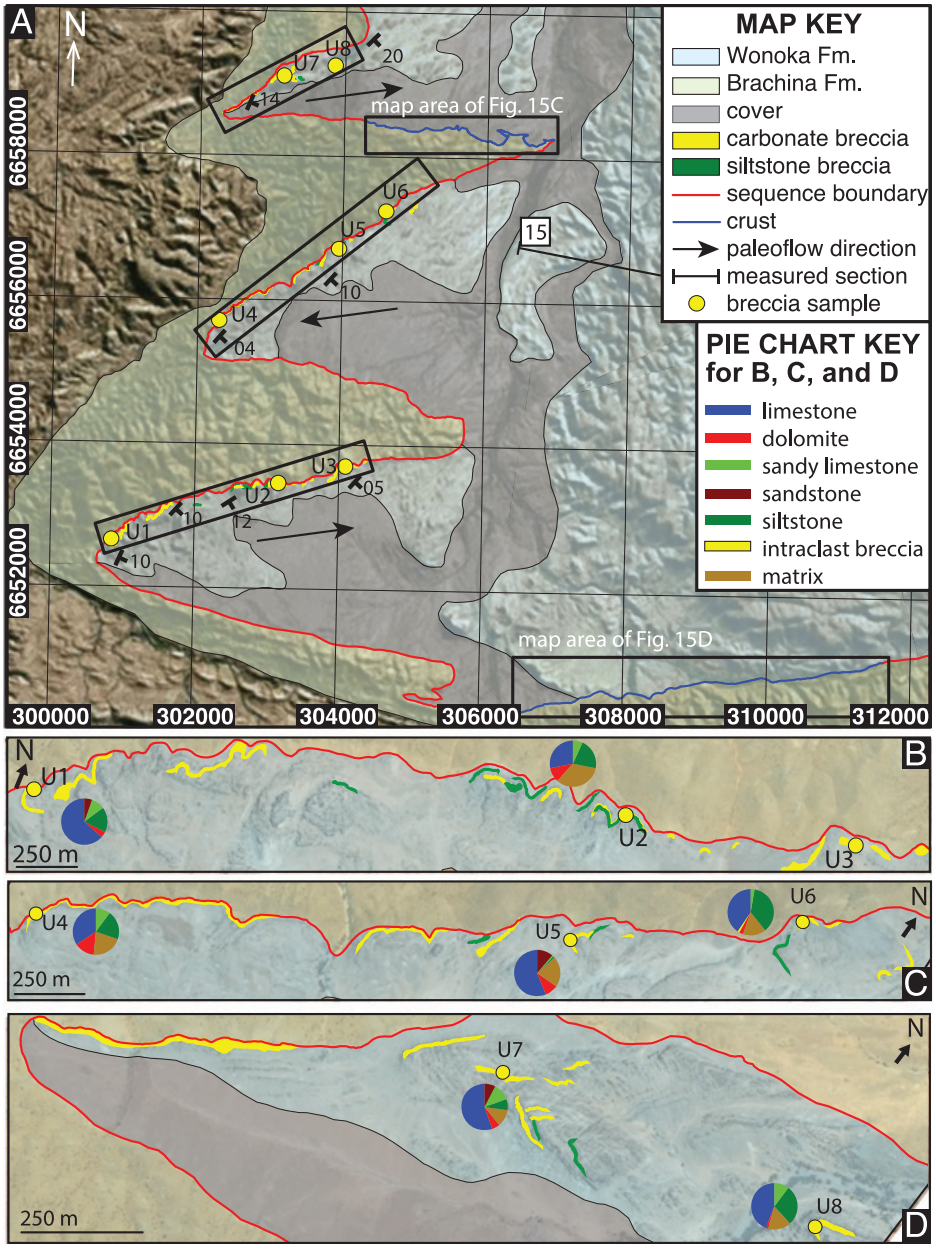

Fig. 9. (A) Geological map of the sinuous, ~1000-m-deep Wonoka paleocanyon at Mount Thomas, with general paleocurrent directions from Eickhoff and others (1988), overlying a Bing Maps aerial photograph (map area marked with white outline on fig. 3A). Map data are displayed as projections onto a Universal Transverse Mercator grid (zone 54S). Red lines indicate the canyon formation sequence boundary, and blue lines mark map areas where this sequence boundary is overlain by carbonate "crust" (see *Canyon-wall Carbonates* section). The insets (B-D) focus on the canyon-fill on the northern walls of the three incisions. In each, debris-flow breccias (figs. 8B-8D), composed primarily of siltstone (mapped as green) or carbonate clasts (mapped as yellow), are most often found near to the Brachina-Wonoka contact. Pie charts depict breccia compositions as measured by clast counting (see Methods for more details).

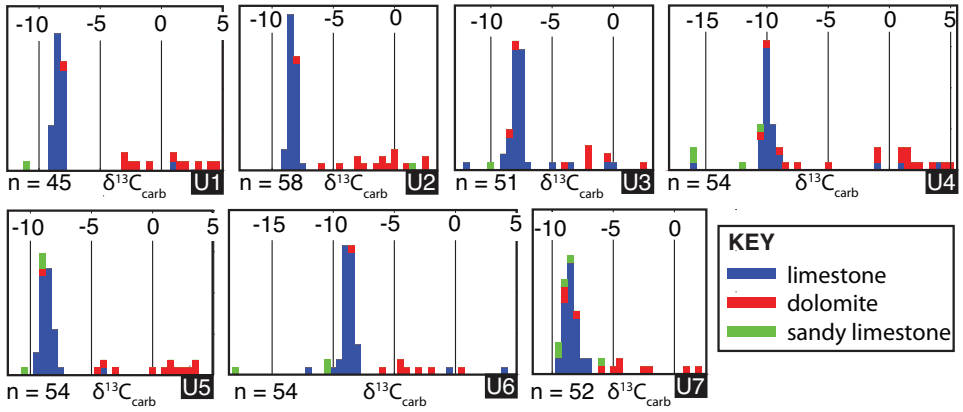

Fig. 10. Relative abundances of $\delta^{13}C_{carb}$ values of the sampled Mount Thomas breccias (U1-U7 on fig. 9). Stacked histograms (bins of isotopic values color-coded as either limestone, dolomite, or sandy limestone) depict fractional abundance of $\delta^{13}C_{carb}$ values of measured clasts (added heights of all bars in a single bar graph equals 1). Though the compositions of carbonate breccias differs dramatically across incisions (see pie charts on figs. 9B–9C), the carbon isotopic distributions of measured clasts are remarkably consistent, and record $\delta^{13}C_{carb}$ values between −12‰ and +5‰.

components were targeted. Samples were slabbed perpendicular to bedding and 5 to 10 milligrams (mg) of powder were micro-drilled from individual laminations for isotopic and trace element analysis. For Mount Thomas and Oodnapanicken canyons, between 50 and 100 clasts from 11 breccia flows were collected in the field, along with measurements of the sampled clasts' long and short axes, color and lithology. Companion clast counts on sampled breccia units were also collected; a 100-point grid on the breccia face was constructed, and at each point, the lithology, long axis, short axis and color of each clast was recorded. For Saint Ronan canyon, hand samples from 16 breccia flows were collected, and, in the lab, powders from individual clasts (15-45 per hand sample) were collected, along with their dimensions, color and lithology.

Samples from sections 6 and 13–15 (fig. 3A) were measured at the University of Michigan Stable Isotope Laboratory. All powders were heated to 200 °C to remove volatile contaminants and water. Samples were then placed in individual borosilicate reaction vessels and reacted at 76 °C with 3 drops of H_3PO_4 on a Finnigan MAT Kiel I preparation device coupled directly to the inlet of a Finnigan MAT 251 triple collector isotope ratio mass spectrometer. All other samples were measured at Princeton University. All powders were heated to 110 °C to remove volatile contaminants and water in individual borosilicate reaction vials. Powders were reacted at 72 °C with 4 to 5 drops of H_3PO_4 on a GasBench II preparation device coupled directly to the inlet of a Thermo DeltaPlus continuous flow isotope ratio mass spectrometer. Precision and accuracy are monitored by running 14 standards for every 72 unknowns. The standard set includes a primary standard (NBS-19) and a secondary, in-house marble standard. $\delta^{13}C$ and $\delta^{18}O$ were acquired simultaneously on both systems, and isotopic data are reported in the standard delta notation as the permil difference from the VPDB standard (Vienna Pee Dee Belemnite). All samples are measured relative to an internal gas standard, and then converted to the VPDB scale using the known composition of NBS-19 ($\delta^{13}C = 1.95$; $\delta^{18}O = -2.20$) following the data reduction schema of Paul and others (2007). Measured precision is 0.05 to 0.1 permil (1σ) for $\delta^{13}C$ and 0.15 to 0.2 permil (1σ) for $\delta^{18}O$.

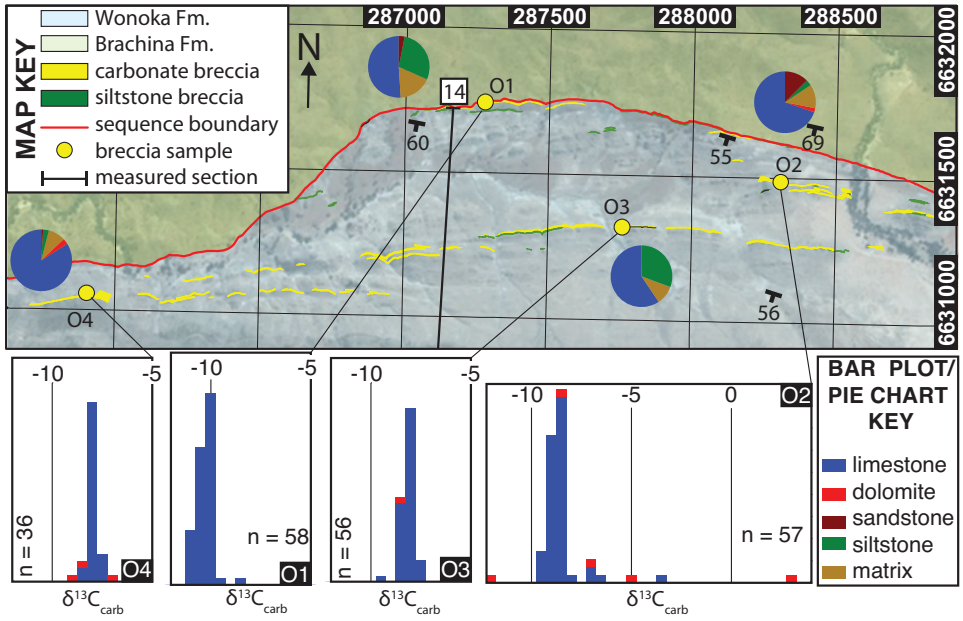

Fig. 11. Geological map of the ~500-m-deep Wonoka paleocanyon at Oodnpanicken overlying a Bing Maps aerial photograph (map area marked with white outline on fig. 3A). Map data are displayed as projections onto a Universal Transverse Mercator grid (zone 54S). Pie chart and histogram symbologies are the same as in figures 9 and 10. Like Mount Thomas, breccias are found near to the Brachina-Wonoka contact (O1); unlike Mount Thomas, breccia flows are also found far from canyon-walls, ~500 m stratigraphically above the deepest part of the incision (O3). There is also much less diversity in breccia composition, with most breccias being dominated by limestone and siltstone clasts and containing very few dolomites. Subsequently, because dolomites carry the most positive $\delta^{13}C_{carb}$ values, the carbon isotopic distributions are also much tighter than at Mount Thomas. Values mostly range between −12 and −7‰, and are remarkably consistent from flow-to-flow across the Oodnapanicken paleocanyon.

Trace Element Abundances

From the micro-drilled powders acquired for $\delta^{13}C_{carb}$-$\delta^{18}O_{carb}$ analysis, a selection of samples were targeted for trace element analysis. 5 mg of each sample were placed in a 15 milliliter (mL) Falcon centrifuge tube along with 5 mL of a buffered solution of anhydrous acetic acid and ammonium hydroxide (pH of ~5) and allowed to react in a sonicator for 5 hours. This style of dissolution is effective in dissolving carbonate phases (both limestone and dolomite), but leaves less soluble sediment phases unleached, such as Fe-Mn oxides and clays (Tessier and others, 1979). Thus, the trace elements released during dissolution are assumed to be carbonate-bound. Each solution was then centrifuged at 2500 rpm for ten minutes. The upper 4 mL of supernatant, clear of any insoluble residue, was pipetted off into another Falcon tube. Before use, every Falcon centrifuge tube was rinsed three times with Millipore Milli-Q filtered water (resistivity: 18.2 MΩ).

Trace element abundances were determined on a Thermo Scientific Element 2 inductively coupled plasma mass spectrometer (ICP-MS). Solutions were diluted with 2 percent HNO_3 acid to set Ca concentrations at 45 to 55 ppm. For each run of 24 unknowns, four multi-element standards, with varying molar ratios of known [element]:[Ca] were also analyzed to develop linear regressions of peak intensity vs. element abundance. Using these regressions, each measured element for the unknowns was projected into [element]:[Ca] (molar ratio) space. All data is reported as ratios of the

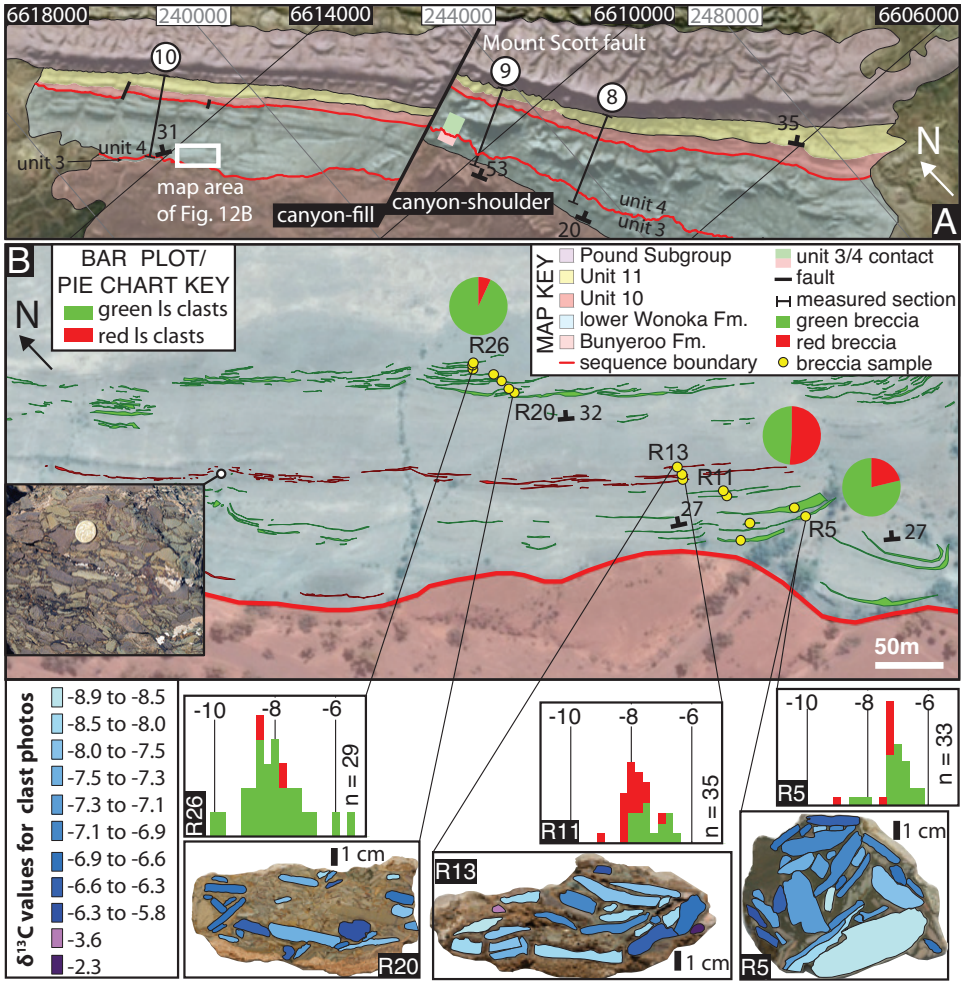

Fig. 12. (A) Geological map of the Saint Ronan canyon-fill and canyon-shoulder complex (map area marked with white outline in fig. 3A). Map data are displayed as projections onto a Universal Transverse Mercator grid (zone 54S). Northwest of the Mount Scott fault, the lowermost ~150 m of Wonoka carbonate (that is, thin event beds interbedded with red siltstone; units 1-3 on fig. 5) are missing, and the Wonoka Fm. sits unconformably on the Bunyeroo Fm. (fig. 3C). Southeast of the fault, on the canyon-shoulder, units 1–3 are preserved, and are capped by intraformational tabular clast breccias (figs. 6D and 6E) and a sharp transition to green siltstone with carbonate interbeds (the "red-to-green" transition; figs. 4 and 5). Field mapping shows that the microbialite reef facies of unit 11, and probably the associated unit 10 siliciclastics, cap both the canyon-fill and canyon-shoulder sequences, thus indicating that canyon cutting and filling occurred before terminal Wonoka deposition. (B) Map of the lower-most canyon-fill stratigraphy, covering the white outline in figure 12A. Breccia units are thin (0.1 to 0.9 m) with little to no matrix, and composed entirely of either red or green limestone clasts. Abundances of each clast color for a selection of sampled flows are shown as pie charts, and stacked histograms of $\delta^{13}C_{carb}$ are also colored by clast color. Clasts range in $\delta^{13}C_{carb}$ value between −9 and −2.5‰, with impressive isotopic variability preserved in even cm-scale hand samples (for example, 3-6‰ on R5, R13, and R20).

measured element [in either millimol (mmol) or micromol (μmol)] against mols of [Ca + Mg]. Normalizing to [Ca + Mg] allows data from limestones and dolomites to be compared meaningfully, as the molar ratio of $[Ca + Mg]/[Ca_xMg_{(1-x)}CO_3] = 1$ for any value of *x*. As our dissolution methods only liberated the carbonate-bound trace

element fractions, the ratios presented can therefore be interpreted as mmol or μmol of an element per mol of carbonate mineral. The one exception to this data presentation scheme is Mg abundance, which is reported as mmol Mg : mol Ca (value of 1000 = stoichiometric dolomite).

To help extract information from these multivariate datasets, principal component analysis (PCA) was performed on the 13 variable data matrix ($\delta^{13}C_{carb}$, $\delta^{18}O_{carb}$, and trace element abundances; n = 247). PCA works to collapse and distill information from multivariate datasets, and potentially identify the number of truly linearly independent variables. PCA defines orthogonal axes, or principal components, along which the variance of a dataset is maximized. The principal components are linear combinations of the different variables; axis orientations are the eigenvectors of the correlation matrix, and the loadings of each variable for each axis are determined by the associated eigenvalue. PCs are ranked by the amount of variance they explain (that is, the 1st PC defines the greatest fraction of total variance, *et cetera*), where for an n-variable dataset, the total variance is n.

Mapping Techniques

Mapping of canyon breccia units at Mount Thomas (fig. 9), Oodnapanicken (fig. 11) and Saint Ronan (fig. 12) was aided by a Trimble differential GPS system. At each mapping location, a stationary base station at a point of high elevation (relative to the mapping area) was established. During a day's work, a Trimble R8 GPS receiver logged the position of the base station every 5 seconds. Mapping was done with a Trimble GeoExplorer 6000 GeoXH handheld device mounted to a 2-m pole and a Tornado external antenna. The coordinates of the basal contact, thickness, and strikes and dips of canyon-fill units were measured and logged on this rover unit. Using the proprietary software Global Pathfinder Office, dispersion in the base station data, caused mainly by atmospheric effects such as cloud cover, was used to correct the rover data. After this differential correction, the precision of 85 percent of the data is < 0.3 m (2σ), with the remaining 15 percent at the 0.3 to 2 m precision level. Larger uncertainties are associated with mapping near cliffs or high rock-walls.

Total Organic Carbon

A subset of Wonoka carbonates (49 from measured section 6, and 23 from measured section 13) were selected to measure total organic carbon abundance (TOC). After removing the outside layer of surface oxidation and large veins, whole rock samples were crushed into powder. Insoluble residues were obtained by acidifying powders in 6N HCl for 24 hours to dissolve all carbonate minerals. The insoluble residues were then rinsed with DI water, dried and loaded into tin capsules for analysis on a GVI Isoprime CF-IRMS linked to a Eurovector elemental analyzer at Rutgers University. Organic carbon concentrations were measured using standards with known carbon concentration and the intensity of masses 44 and 28; standards were run following eight sample unknowns. TOC values (in weight %) for the bulk samples were calculated by combining the carbon concentration data with measurements of the ratio of insoluble residue to original pre-decarbonated powder.

RESULTS

Canyon-shoulder Chemostratigraphy

The $\delta^{13}C_{carb}$ profiles of 12 measured canyon-shoulder sections, dispersed across ~12,000 km^2 of ARC basin map area, are remarkably consistent from section to section (figs. 4 and 5). A composite Wonoka physical- and chemo-stratigraphy, with all the individual sections stretched to account for variations in canyon-shoulder thickness across the ARC (between 500 and 850 m), is shown in figures 13A to 13C. For half the

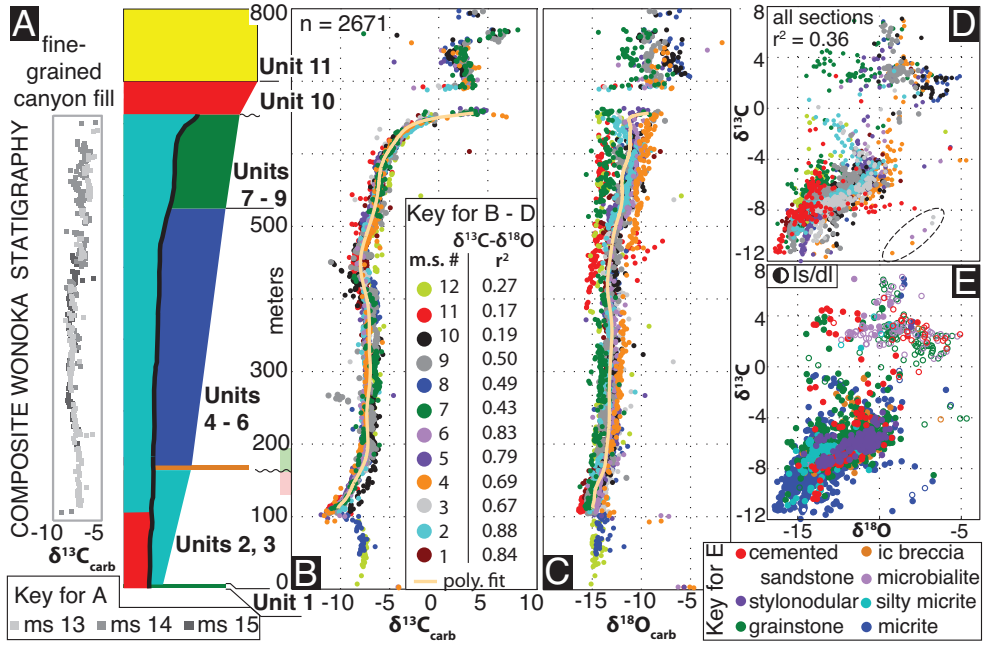

Fig. 13. (A) Composite canyon-fill (left-side of the stratigraphic column, separated by thick black line) and canyon-shoulder lithostratigraphy (right-side of the stratigraphic column), with $\delta^{13}C_{carb}$ of fine-grained canyon-fill from Mount Goddard, Oodnapanicken and Mount Thomas paleocanyons (measured sections 13, 14 and 15 on fig. 3A). By accounting for the variable thickness of canyon-shoulder sections across the ARC (~500 to 850 m), composite $\delta^{13}C_{carb}$ (B) and $\delta^{18}O_{carb}$ (C) profiles for the Wonoka Fm. canyon-shoulder can be constructed. A degree 20 polynomial curve, designed to describe the smoothed, general isotopic evolution of the Wonoka canyon-shoulder, is fit to both profiles, and used to compare isotopic offsets between sections (see fig. 19). $\delta^{13}C_{carb}$-$\delta^{18}O_{carb}$ cross plot showing data from all canyon-shoulder sections, coded by lithology ("ls" stands for limestone; "dl" for dolomite) and section number (D) and by lithology and lithofacies (E). All r^2 values displayed on this figure are calculated for $\delta^{13}C$ values less than −5‰, and p values are all less than 0.001. In general, canyon-shoulder sections do show $\delta^{13}C_{carb}$-$\delta^{18}O_{carb}$ correlation, though the correlation is often stronger when the data is divided by section (for all data compiled, $r^2 = 0.36$ for $\delta^{13}C_{carb} < -5‰$, compared to the chart in panel (B), where individual section r^2 values reach 0.88). Six outliers were excluded (out of 2201 total for all sections) from these r^2 calculations – 2 data points each from sections 3, 4, and 6 – and are circled with a dashed ellipse. In the key for panel (E), lithofacies are organized in order of increasing permeability (that is, ranging from fine-grained micritic wavy laminites to coarse grainstones and sandy carbonates). No pattern of dependence between isotopic values and lithofacies is observed.

measured sections, the stratigraphically lowest Wonoka carbonates hold the most negative $\delta^{13}C_{carb}$ values (the nadir ranges from −12 to −10‰). The exceptions are (a) measured sections with the 10 cm Wearing dolomite, which has variable $\delta^{13}C_{carb}$ values (between −5 and −3‰), and (b) measured sections 8 and 12 (fig. 5), where basal carbonates are ~ −7.5 permil, and drop to nadir values of −10 permil over 50 to 100 m. From the nadir, the $\delta^{13}C_{carb}$ profiles recover smoothly over 100 to 150 m (unit 3) to a stable, plateau value. The following 300 to 400 m of middle Wonoka stratigraphy, beginning in most sections with the transition from red-to-green siltstone (measured sections 1, 3, 5, 7, 9 and 11 on figs. 4 and 5), is host to these relatively invariant $\delta^{13}C_{carb}$ values, ranging from −8 to −7 permil (units 4-6). This stratigraphic interval of stability ends with a smooth rise in $\delta^{13}C_{carb}$ from the plateau value towards 0 permil over 150 to 200 m. The $\delta^{13}C_{carb}$ profiles cross 0 permil near the top of unit 8; when present, unit 9 carbonates are always positive (between +2 and +5‰). After the recovery to positive values, the $\delta^{13}C_{carb}$ record is interrupted by 30 to 150 m of

siliciclastics (unit 10). The final portion of the Wonoka $\delta^{13}C_{carb}$ profile is represented by the unit 11 microbialites, which are always positive and range between +2 and +8 permil.

One common, but not universal, attribute of Ediacaran carbonate successions which host the Shuram excursion is strong covariation between $\delta^{13}C_{carb}$ and $\delta^{18}O_{carb}$, especially for samples with $\delta^{13}C_{carb} < -5$ permil (fig. 1D). Our canyon-shoulder data share this attribute, especially for sections 1–9 (key on fig. 13B). When plotted as a stratigraphic composite, however, $\delta^{18}O_{carb}$ values from section to section do not display the same consistency as $\delta^{13}C_{carb}$ values, with offsets between sections of 5–6 permil (fig. 13C). As a result, data compiled from all sections do not show as strong a correlation between $\delta^{13}C_{carb}$ and $\delta^{18}O_{carb}$ compared to data from individual sections ($r^2 = 0.36$ for all sections combined for $\delta^{13}C_{carb} < -5$ permil, whereas individual sections have r^2 values as high as 0.88; fig. 13D). The combined r^2 value is somewhat higher (0.45) if sections 10–12 are excluded, which display the poorest correlations between $\delta^{13}C_{carb}$ and $\delta^{18}O_{carb}$.

Canyon-fill chemostratigraphy is markedly different from the canyon-shoulders. At Oodnapanicken and Mount Thomas paleocanyons (sections 14 and 15, respectively, on fig. 3A), the lower half of most canyon-fill sections is carbonate poor, except for tabular–clast carbonate breccias near the base (figs. 8B-8D). Fine-grained, wavy-laminated carbonate beds (hereafter referred to as the "fine-grained canyon-fill") become abundant above 300 to 400 m of basal canyon-fill. At the shallower Mount Goddard paleocanyon (section 13 on fig. 3A), the canyon-fill sequence is composed entirely of this facies. The $\delta^{13}C_{carb}$ profile of the fine-grained canyon-fill is less variable, when compared to the canyon-shoulder; values range between −8 and −6 permil (fig. 13A). The fine-grained canyon-fill therefore does not record the extremely depleted $\delta^{13}C_{carb}$ values (down to −12‰) seen in the canyon-shoulders nor the return to positive $\delta^{13}C_{carb}$ values. Furthermore, correlation between $\delta^{13}C_{carb}$ and $\delta^{18}O_{carb}$ is non-existent ($r^2 = 0.003$ and $p = 0.285$ for sections 13-15 combined).

Isotope Conglomerate Tests

In direct analogy to a paleomagnetic conglomerate test, wherein clasts recording random magnetic directions within a conglomeratic unit constitutes a "pass" and is indicative of primary magnetization, Husson and others (2012) introduced an *isotope conglomerate test* to the study of Wonoka Fm. chemostratigraphy. Husson and others (2012) measured $\delta^{13}C_{carb}$ and $\delta^{18}O_{carb}$ values on clasts from the breccia units of Mount Thomas, Oodnapanicken, and Saint Ronan canyon-fill sections (figs. 9, 11, and 12, respectively) to assess provenance and relative timing of isotopic acquisition [for example, DeCelles and others (2007)]. Here we corroborate the findings of Husson and others (2012) with an additional 908 isotopic measurements of clasts from breccia units of Mount Thomas, Oodnapanicken, and Saint Ronan paleocanyons; the tripling of the clast isotopic dataset from Husson and others (2012) also allows for more rigorous assessment of (a) potential clast sources feeding the Wonoka breccias, (b) how clast $\delta^{13}C_{carb}$ values change from flow-to-flow and canyon-to-canyon and (c) how the isotopic distributions compares between breccia flows and canyon-shoulder profiles. Summary results are shown in figure 14.

At Mount Thomas (fig. 9) and Oodnapanicken (fig. 11), breccia units range from 0.1 to 30 m thick, are clast-supported in a matrix of fine sand, and consist primarily of siltstone, sandstone, sandy limestone, and 1 to 100 cm long carbonate clasts of two dominant lithologies: gray, micritic limestone and brown dolostone. Moving along strike from the edges towards the middle of their exposures, breccia units thicken, mostly by 1 to 2 m, and more rarely by 5 to 8 m. The most dramatic example of thickening is found at Oodnapanicken (O4 on fig. 11), where a 4 m breccia unit rapidly thickens to 30 m over 25 m of along-strike distance. At Mount Thomas, the

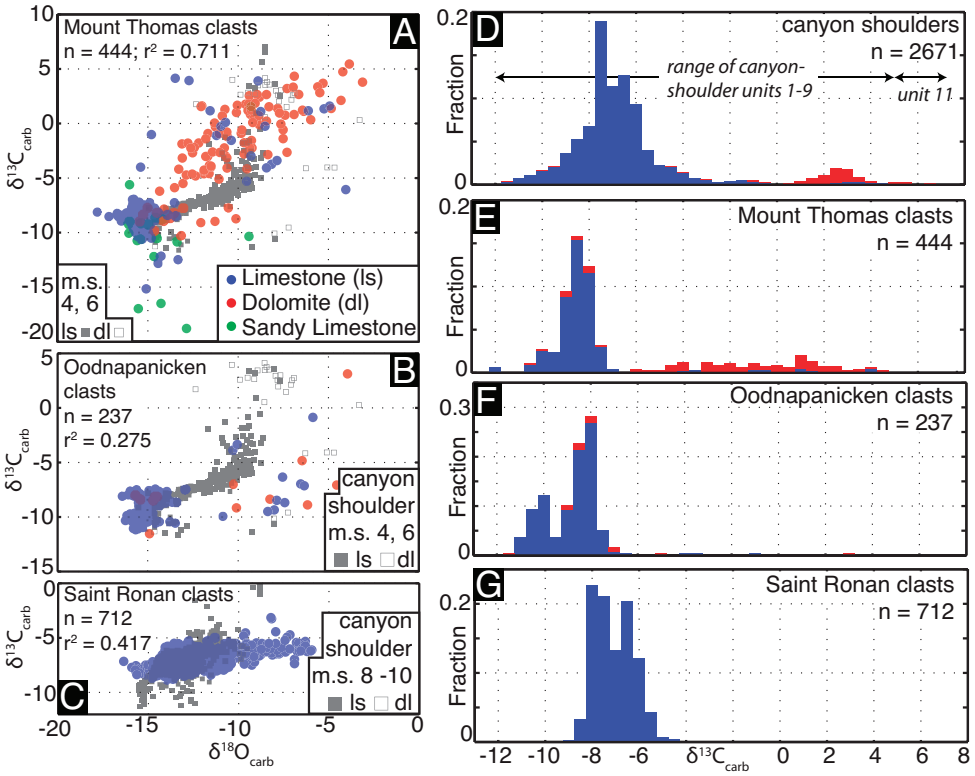

Fig. 14. Summary of results of isotope conglomerate tests from Mount Thomas (A; see figs. 9 and 10), Oodnapanicken (B; see fig. 11) and Saint Ronan (C; see fig. 12) paleocanyons. For comparison, the $\delta^{13}C_{carb}$-$\delta^{18}O_{carb}$ data from sections 4 and 6 canyon-shoulders (dark gray squares) are plotted in the background of (A) and (B). For panel (C), the $\delta^{13}C_{carb}$-$\delta^{18}O_{carb}$ data from units 1–8 of the immediately adjacent canyon-shoulder sections (measured sections 8–10 on fig. 5) are plotted in the background. The clasts of the more distal, Oodnapanicken and Mount Thomas canyon-fill exhibit the full range of $\delta^{13}C_{carb}$ values observed in units 1–9 in canyon-shoulder sections throughout the basin (figs. 4, 5 and 13B). Relative abundances of $\delta^{13}C_{carb}$ in 0.5‰ bins color coded by lithology (blue = limestone; red = dolomite) for the compiled canyon-shoulder dataset (D), and the breccia units of Mount Thomas (E), Oodnapanicken (F) and Saint Ronan (G).

$\delta^{13}C_{carb}$ distributions of 7 distinct breccia units are remarkably consistent across the outcrop area (fig. 10), despite differing breccia compositions as measured by clast counting (figs. 9B-9D). The consistency in distributions is evidence against the presence of significant sampling biases in our field collections (or, if biases existed, they were uniformly present during all sampling sessions). Individual breccia units have $\delta^{13}C_{carb}$ values ranging from −12 to +5 permil, and show strong and significant $\delta^{13}C_{carb}$-$\delta^{18}O_{carb}$ correlation (fig. 14A). Most clast values range from −9 and −7 permil. Values above −5 permil are more rare, and are found mostly in the dolomite clasts (fig. 10). The breccia units of Oodnapnicken are dominated by limestone clasts (constituting 50-75% of each clast count; fig. 11). Dolomite clasts are much more rare at Oodnpanicken than at Mount Thomas, and consequently Oodnapanicken breccia units have much tighter $\delta^{13}C_{carb}$ distributions (fig. 11). With 4 breccia units analyzed, almost all Oodnapanicken clasts have $\delta^{13}C_{carb}$ values ranging from −12 to −7 permil, with only five samples above −5 permil and one with a value above 0 permil (out of 237 Oodnapanicken clasts; figs. 11 and 14B).

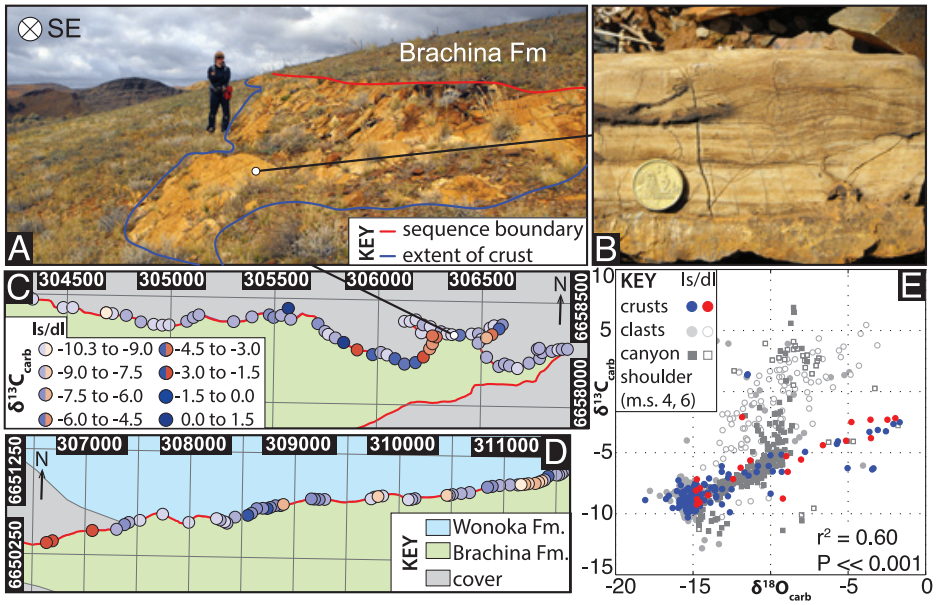

Fig. 15. Field (A) and hand sample (B) photographs of the carbonate "crust" overlying the paleocanyon wall at Mount Thomas (fig. 9A). (C, D) Locations of samples of in-place crust, marked by dots and coded by lithology (blue colors for limestone, red colors for dolomite) and $\delta^{13}C_{carb}$ value (lighter tone = more negative $\delta^{13}C_{carb}$) were taken along two exposure belts at Mount Thomas. The map data are displayed as projections onto a Universal Transverse Mercator grid (zone 54S). (E) Crust carbonate varies between −10.3 and 1.5‰ with no discernible geographic pattern, but with very strong $\delta^{13}C_{carb}$-$\delta^{18}O_{carb}$ correlation. The large $\delta^{13}C_{carb}$-$\delta^{18}O_{carb}$ range of carbonate crust makes it a potential source of limestone and dolomite clasts for debris flow breccias deposited in nearby canyon-fill sequences. For comparison, the $\delta^{13}C_{carb}$-$\delta^{18}O_{carb}$ data from Mount Thomas breccia clasts (light gray) and canyon-shoulder sections 4 and 6 (dark gray) are plotted in the background.

The breccia units of Saint Ronan (fig. 12) are distinctly different from those of Mount Thomas and Oodnapnicken. Breccia flows are thinner, ranging from 0.1 to 0.9 m over the mapped area (fig. 12B). Saint Ronan breccias lack dolomite, sandy limestone, sandstone, and siltstone and contain little matrix; clast populations instead consist entirely of either red or green wavy laminites and coarser grainstones. Like Oodnapanicken, the $\delta^{13}C_{carb}$ distributions of breccia units are tighter than Mount Thomas, though values do not get as negative (observed range is −9 to −2.5‰) as compared to other paleocanyon sites. Thus, the $\delta^{13}C_{carb}$ range of canyon-shoulder units 1–9 (−12 to +5‰; fig. 14D) is seen in the breccia units of the more distal canyon-fill of Mount Thomas and Oodnapanicken, with the full range best expressed in Mount Thomas (fig. 14E). The breccias of the more proximal Saint Ronan, while lacking the full $\delta^{13}C_{carb}$ range seen in units 1–9 (fig. 14G), still show considerable variability within single breccia units (6‰ is the maximum range, with 3 to 4‰ being the average range; R5, R11, R13, R20 and R26 on fig. 12).

Canyon-wall Carbonates

In certain paleocanyons, 0.05 to 5 m thick gray-to-yellow micritic carbonate layers are found directly above the canyon wall surface (figs. 8A, 9A and 15A, 15B), often at orientations significantly discordant with either the underlying Brachina Fm. or overlying Wonoka canyon-fill sediments (fig. 9A). Locally, the layer is partially-to-fully dolomitized, and browner in color. These beds are of a controversial origin. Eickhoff

and others (1988) cited its negative $\delta^{13}C_{carb}$ and $\delta^{18}O_{carb}$ values (from −9 to −8‰ and −16 to −15‰, respectively, on 5 samples) to argue for a non-marine origin. Specifically, Eickhoff and others (1988) interpreted the layer as a tufa "crust", an interpretation that supported their model of subaerial exposure driving canyon formation. In contrast, Giddings and others (2010), noting that canyon-shoulder carbonates of the Wonoka Fm. share similar isotopic values, argued that these crusts formed in a marine setting and were microbially mediated, forming during periods of low sedimentation rates in the Wonoka canyons. These "crusts" are found at the Mount Thomas paleocanyon and at the Patsy Spring paleocanyon [15 km from Oodnapanicken (Giddings and others, 2010)], but are not observed at Saint Ronan.

Samples of *in-situ* crust were collected above the canyon wall at Mount Thomas (figs. 9A and 15C–15D). In map view, no spatial pattern in either $\delta^{13}C_{carb}$ value or lithology (limestone vs dolomite) of the crust is observed (figs. 15C-15D). $\delta^{13}C_{carb}$ values range from −10.3 to +1.5 permil, and correlate strongly and significantly with $\delta^{18}O_{carb}$ (fig. 15E). Thus, given their proximity, their similarity in lithofacies and their isotopic overlap, there is reason to suspect that crust limestone and dolomite are sources for the Mount Thomas and Oodnapnicken breccia units, though differences are apparent. For example, crust limestones and dolomites overlap in $\delta^{13}C_{carb}$-$\delta^{18}O_{carb}$ space (fig. 15E), and thus, unlike Mount Thomas and Oodnapanicken clasts, are not strongly sorted isotopically by lithology (figs. 14A and 14B). It is unlikely that the crusts were a source to the Saint Ronan breccia units, which lack dolomites and whose clasts are identical in appearance to limestones (units 1-8) from the adjacent canyon-shoulder strata (measured sections 8-10 on figs. 5 and 12A).

Trace Element Abundances

In order to better assess which sources were active in feeding the Mount Thomas, Oodnapanicken and Saint Ronan breccia units, samples representing the canyon-shoulder, fine-grained canyonfill, crusts, and clast populations were selected for trace element analysis. Trace element data are reported as molar ratios—either mmol or μmol of a particular element X over mols of [Ca +Mg] in the measured sample. As our dissolution protocol only targets carbonate phases, these ratios can be described as the mmol or μmol abundance of an element per mol of carbonate mineral. Abundances of 11 elements (Al, Fe, Mn, K, Na, Mg, Sr, Th, Li, U and V) are plotted against $\delta^{13}C_{carb}$ values in figure 16. Visually, most populations overlap. One exception are the Mount Thomas clasts, which have the highest Mg abundances; this observation is consistent with a greater abundance of dolomite over a large range in $\delta^{13}C_{carb}$ values as compared to other Wonoka carbonate populations (fig. 14E). The most striking trend seen in these 11 cross-plots is that crust samples often have the highest metal abundances, especially in [Al], [Mn], [K], [Na], and [Li]. While dolomite clasts and canyon-shoulder horizons have the highest Mg abundances, crust samples display a range of intermediate [Mg] values not seen in the other datasets.

Geochemistry of Stylonodular Beds

In both canyon-fill and canyon-shoulder sections, primary sedimentary fabrics in the Wonoka Fm. are well preserved (figs. 6E-6I, 6K, 6L and 8B-8F). The one obvious exception is stylonodular bedding (fig. 7), a fabric destructive, diagenetic texture that is well developed over 50 to 200 m of middle Wonoka canyon-shoulder stratigraphy (figs. 4 and 5). Although contacts between well-preserved grainstones and stylonodular beds are most often sharp (figs. 7B and 7D), diffuse contacts of upwardly increasing nodule size do exist, wherein grainstone gradually becomes stylonodular over 5 to 10 cm of upward vertical distance (fig. 7C). The texture emanates from bed-tops downward and is most likely associated with sedimentation hiatuses and hard ground formation (Haines, 1988).

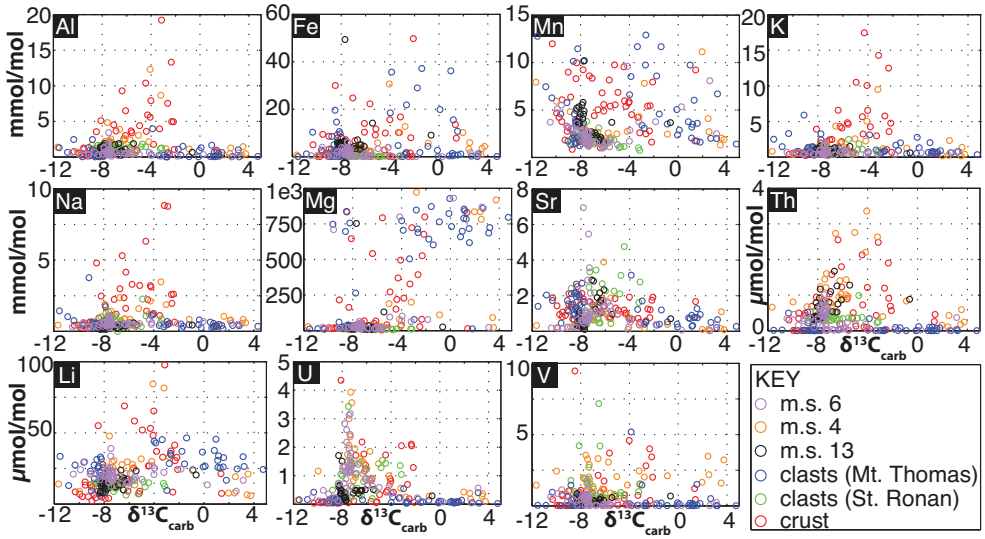

Fig. 16. In order to further constrain possible sources of carbonate for canyon-fill breccias (figs. 8B-8D), 247 samples covering the full suite of different Wonoka carbonates [canyon-shoulder (measured sections 6 and 4 on fig. 4), fine-grained canyon-fill (measured section 13 on fig. 3A), Mount Thomas clasts (fig. 9), Saint Ronan clasts (fig. 12) and crusts (fig. 15)] were selected for trace element analysis. The abundances of 11 metals are expressed as molar ratios, in either mmol or μmol/mol [Ca + Mg]. The exception is Mg, which is expressed as mmol/mol Ca. Molar ratios are plotted here against $\delta^{13}C_{carb}$ value.

To investigate whether there are any preserved geochemical signals of this diagenesis, a transect across a 5 cm grainstone-to-stylonodular transition was micro-drilled at 1 to 2 mm resolution (fig. 17), and analyzed for $\delta^{13}C_{carb}$, $\delta^{18}O_{carb}$ and trace element abundances. As the grainstone texture becomes progressively destroyed, $\delta^{13}C_{carb}$ drops by ~0.4 permil, and [Fe] and [Mn] increases (figs. 17A, 17C and 17D). [Mg] increases until 1.75 cm below the bed-top (fig. 17E); the trend in [Fe] also is much better preserved over this same interval. $\delta^{18}O_{carb}$ is not correlated with this sedimentary transformation (fig. 17B). These trends are consistent with recrystallization of carbonate in the presence of a Fe- and Mn-rich, $\delta^{13}C_{carb}$ depleted fluid (relative to its initial composition; in this case, −5.8‰), resulting in < 0.5 permil shifts in $\delta^{13}C_{carb}$. These geochemical trends are also consistent with many studies of carbonate diagenesis, which often show similar correlations between [Fe], [Mn], and $\delta^{13}C_{carb}$ [for example, Pingitore Jr (1978); Allan and Matthews (1982); Banner and Hanson (1990); Jacobsen and Kaufman (1999)].

DISCUSSION

Basin Scale Geochemical Signals—Trace Elements

In order to search for mechanisms driving the observed distribution of trace elements, principal component analysis was performed on the Wonoka dataset (see *Trace Element Abundances* section). The 1st PC (32% of total variance) contains loadings that are all positive, except for Sr abundance, with no clear dominant factor (fig. 18A). Projections (also known as *scores*) along PC 1 are thus a weighted mean of all variables (except for [Sr]) for each sample. In other words, positive factors mean that a high value for a particular variable (relative to the mean of the full Wonoka dataset for that particular variable) will contribute constructively to an overall higher PC 1 score; for example, a sample with overall high metal abundances will plot positively in the PC 1.

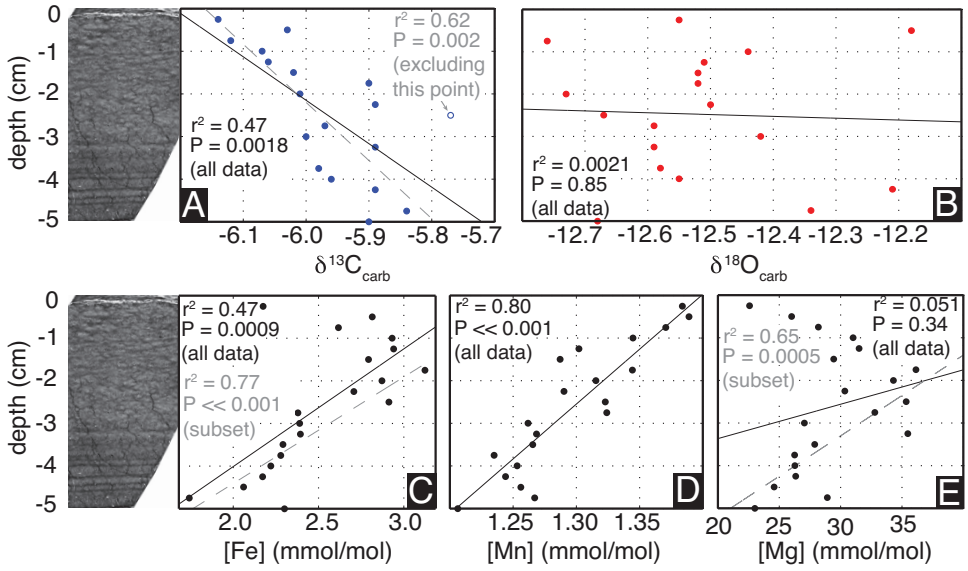

Fig. 17. To investigate the geochemical effects of nodular bed formation, a 5-cm transect covering a gradual contact between well-preserved, laminated grainstone to a fully nodular bed-top (note the upwardly increasing nodule size), was microdrilled every ~ 25 mm. Increasing degree of primary fabric destruction is associated with a ~ 0.4‰ drop in $\delta^{13}C_{carb}$ (A) but no trend in $\delta^{18}O_{carb}$ is observed along the transect length (B). The isotopic drop in $\delta^{13}C_{carb}$ is accompanied by increases in the abundances of Fe (C), Mn (D), and Mg (E), though in the case of Mg, the correlation reverses 1.75 cm below the transect top. In the cross-plots, solid black lines represent linear fits through the full dataset (accompanied with r^2 and p values, also in black), while dashed gray lines, where present, represent fits through subsets of the data displayed (associated r^2 and p values in gray; for C and E, the selected subset is for data between −5 and −1.75 cm depth).

For the 2nd PC (18% of total variance), $\delta^{13}C_{carb}$, $\delta^{18}O_{carb}$, [Fe], [Mg] and [Mn] have the largest positive loadings, and [Th] and [U] have the largest negative loadings. An appropriate geochemical mechanism to describe PC 2 must therefore result in positive correlations between $\delta^{13}C_{carb}$, $\delta^{18}O_{carb}$, [Fe], [Mg] and [Mn] (at least in the context of the Wonoka dataset). PC 2 values are therefore consistent with dolomitization, where the difference in distribution coefficients between calcite and dolomites are consistent with increases in [Fe] and [Mn] (and, obviously, [Mg]) and decreases in [Sr] (Kretz, 1982). Decreasing [U] is sensible if the dolomite formed under reducing conditions [as is common today; Baker and Kastner (1981)], given that oxidized U^{6+} is dramatically more soluble than the reduced form U^{4+} (Barnes and Cochran, 1990). The positive loadings of $\delta^{13}C_{carb}$ and $\delta^{18}O_{carb}$ in PC 2 are sensible given that Wonoka dolomites are at the top of the stratigraphic sections (figs. 13B and 13C) and carry the most positive $\delta^{13}C_{carb}$-$\delta^{18}O_{carb}$ values (figs. 14D-14F and 15C-15E). The 3rd PC (11% of total variance) has 4 important coefficients: negative loadings for $\delta^{13}C_{carb}$ and $\delta^{18}O_{carb}$, and positive loadings for [Fe] and [Mn]. Similar geochemical correlations are observed in the sampling transect crossing the transformation to a stylonodular bed (See *Geochemistry of Stylonodular Beds* section and fig. 17). Thus, this PC is consistent with diagenesis in the style of stylonodular bed formation, resulting in a lowering of $\delta^{13}C_{carb}$ and $\delta^{18}O_{carb}$ and an increase in [Fe] and [Mn] (Banner and Hanson, 1990; Jacobsen and Kaufman, 1999).

Together, these three PCs account for 61 percent of the total variance, and cross-plots of 1st PC versus 2nd PC scores and 2nd PC versus 3rd PC scores are shown in figures 18D and 18E. As in the trace element plots (fig. 16), the crusts stand out from

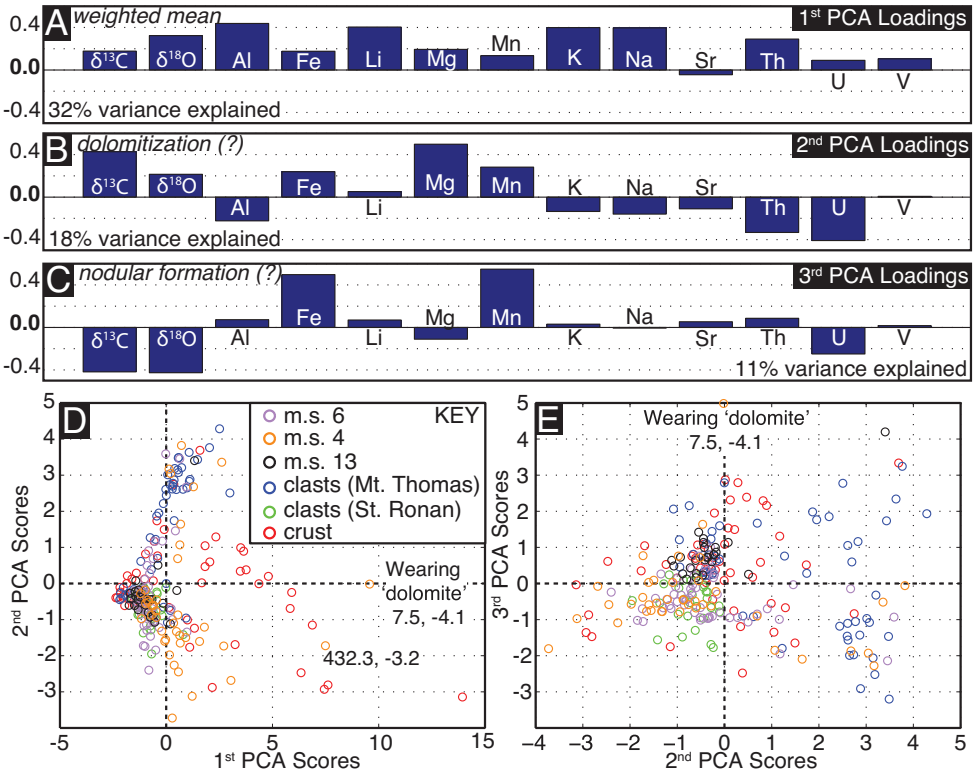

Fig. 18. To better extract information from the multivariate dataset presented in figure 16, principal component analysis was performed on the 13 variable dataset ($\delta^{13}C_{carb}$, $\delta^{18}O_{carb}$, and trace element abundances; n = 247). (A-C) Principal component coefficients are shown as bar plots for the 1st, 2nd, and 3rd principal component axes, respectively. Using these coefficients, the data can be projected onto the new axes, and cross-plots of 1st PC vs. 2nd PC scores and 2nd PC vs. 3rd PC scores, color-coded by sample type, are shown in (D) and (E), respectively. Outliers from the section 4 sample suite (fig. 4) are labeled with their stratigraphic height and $\delta^{13}C_{carb}$ value.

other Wonoka samples. In PC 1, their scores are split between positive and negative values, whereas canyon-shoulder (measured sections 6 and 4 on fig. 4) and clasts plot mostly negative (fig. 18D). As these different pools of carbonates overlap in $\delta^{13}C_{carb}$ and $\delta^{18}O_{carb}$ values (fig. 15E), differences in PC 1 scores must be driven by metal abundances, implying that crust samples have higher than average metal abundances (fig. 16). In PC 2, the largest outliers are the Mount Thomas clasts data, which plot positive relative to all other Wonoka carbonates (figs. 18D and 18E). If PC 2 scores correlate with dolomitization (higher scores = more fully dolomitized), then this pattern is consistent with the greater abundance of dolomites in the Mount Thomas clast dataset over a large $\delta^{13}C_{carb}$-$\delta^{18}O_{carb}$ range (fig. 14E).

Basin Scale Geochemical Signals—$\delta^{13}C_{carb}$ and $\delta^{18}O_{carb}$ Values

Are the signals of diagenetic alteration associated with stylonodular bed formation (fig. 17) seen in the larger canyon-shoulder $\delta^{13}C_{carb}$-$\delta^{18}O_{carb}$ dataset (figs. 4, 5 and 13)? To assess this possibility, the composite $\delta^{13}C_{carb}$ and $\delta^{18}O_{carb}$ profile was fit with a degree 20 polynomial curve, designed to capture the smoothed, basin-wide isotopic signals expressed in the ARC (figs. 13B and 13C). For a given section, the "predicted"

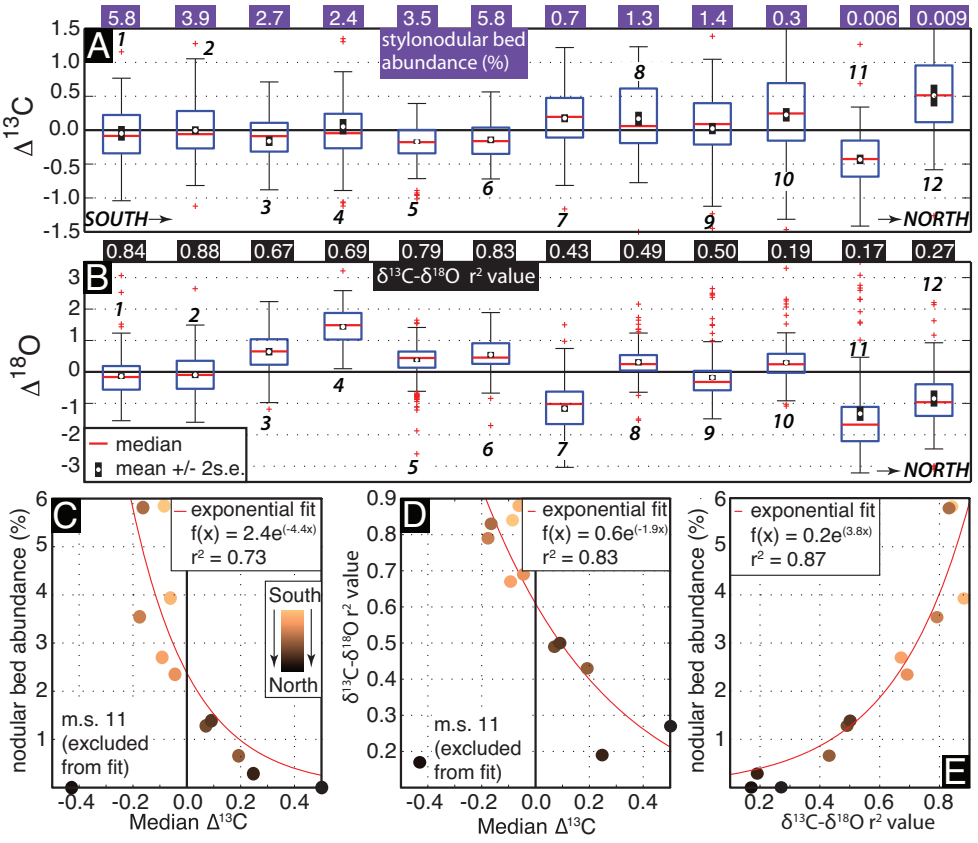

Fig. 19. To examine isotopic differences between the 12 canyon-shoulder sections, the measured $\delta^{13}C_{carb}$ and $\delta^{18}O_{carb}$ values from each section were compared to the "predicted" isotopic values, as expressed by the polynomial fit to the composite $\delta^{13}C_{carb}$ and $\delta^{18}O_{carb}$ profiles (figs. 13B and 13C). The "predicted" value was subtracted from the observed value, creating a dataset of $\delta^{13}C_{carb}$ deviations ($\Delta^{13}C$) and $\delta^{18}O_{carb}$ deviations ($\Delta^{18}O$) for each measured section. Box-whisker plots, with red lines representing the median value and the white circle with black bounds representing the mean ± 2 standard errors of $\delta^{13}C$ and $\Delta^{18}O$ distributions are plotted by section number in (A) and (B), respectively. In most instances, mean overlaps with the median; thus, the distributions are broadly Gaussian. Also displayed are the abundances of stylonodular bedding, measured as [total thickness of nodular beds] / [total section thickness] × 100 in (A) and the $\delta^{13}C_{carb}$-$\delta^{18}O_{carb}$ r^2 values (for $\delta^{13}C_{carb} < -5‰$) for each section in (B). Plots of median $\delta^{13}C$ value for each section vs. nodular bed abundance (C) and median $\delta^{13}C$ value vs. $\delta^{13}C_{carb}$-$\delta^{18}O_{carb}$ r^2 value (D), both of which display strong negative correlations, especially when data from section 11 are excluded. This section is not an outlier, however, when a section's nodular bed abundance is plotted against its $\delta^{13}C_{carb}$-$\delta^{18}O_{carb}$ r^2 value (E).

$\delta^{13}C_{carb}$ and $\delta^{18}O_{carb}$ (calculated via the polynomial fit) was subtracted from the measured $\delta^{13}C_{carb}$ and $\delta^{18}O_{carb}$ for all sampled horizons. These deviations in $\delta^{13}C_{carb}$ ($\Delta^{13}C$) and $\delta^{18}O_{carb}$ ($\Delta^{18}O$) are displayed in box-whisker plots by section in figures 19A and 19B, with the red lines denoting the median $\Delta^{13}C$ and $\Delta^{18}O$ value for each section and the white circles with black bounds denoting the mean ±2 standard errors (s.e.). The variability of $\Delta^{13}C$ is smaller than $\Delta^{18}O$ (median $\Delta^{13}C$ values range from −0.5 to +0.5‰, whereas median $\Delta^{18}O$ values from −2 to +1.5‰). Furthermore, there is a discernible geographic pattern in $\Delta^{13}C$ (fig. 19A), with the six southernmost sections being negative in $\Delta^{13}C$ (median $\Delta^{13}C$ ranges form −0.2 to −0.1‰) and five northern sections being positive (median $\Delta^{13}C$ ranges from +0.05 to +0.5‰). The one

exception to this basin sorting is measured section 11 (fig. 5), which has the most negative median $\Delta^{13}C$ value (−0.5‰). In contrast, the larger amplitude changes in $\Delta^{18}O$ values do not exhibit any obvious geographic patterns (fig. 19B).

Excellent correlations also exist between median $\Delta^{13}C$ and other section metrics. There is a negative correlation between median $\Delta^{13}C$ and the abundance of stylonodular beds at each section (expressed as [total thickness of stylonodular beds]/[total Wonoka section thickness] × 100; fig. 19C). The relationship appears to be exponential, with the effect of stylonodular bed abundance on $\Delta^{13}C$ saturating above ~6 to 7 percent nodular bed occurrence; the fit in figure 19C excludes section 11, which has the lowest median $\Delta^{13}C$ and almost no stylonodular beds. A similar, negative correlation also exists between median $\Delta^{13}C$ value and the strength of $\delta^{13}C_{carb}$-$\delta^{18}O_{carb}$ covariation at each section (measured as the r^2 value between $\delta^{13}C_{carb}$ and $\delta^{18}O_{carb}$ for $\delta^{13}C_{carb} < -5$‰; fig. 19D). Finally, the strongest correlation, and one that does not require the exclusion of data from section 11, is a positive correlation between stylonodular bed abundance and $\delta^{13}C_{carb}$-$^{18}O_{carb}$ covariation strength (fig. 19E). The geochemical effect of stylonodular bed formation shares a similar isotopic scale with $\Delta^{13}C$ values; a drop of 0.3 to 0.4 permil is observed across a diffuse well-preserved to fully nodular transition, and differences between median $\Delta^{13}C$ are ~0.6 permil. The isotopic scale of $\delta^{13}C_{carb}$-$\delta^{18}O_{carb}$ covariation, however, is much larger, occurring in most canyon-shoulder carbonates with $\delta^{13}C_{carb}$ values of −12 to −5 permil (fig. 13D). Thus, a causal connection between section r^2 values and these other section metrics is not immediately apparent.

Constraints from Isotope Conglomerate Tests

In the Ediacaran-aged Wonoka Formation of South Australia, a deep negative excursion in $\delta^{13}C_{carb}$ evolves from −12 to +5 permil over ~700 m of canyon-shoulder stratigraphy. The chemo- and lithostratigraphies of canyon-shoulder sections are remarkably consistent across 12,000 km^2 of basin area (figs. 4, 5 and 13B), with our physical stratigraphic observations congruous with the unit framework established by Haines (1990). Differences between $\delta^{13}C_{carb}$ profiles of measured sections exist, although offsets between sections are small, and mostly range between 0.5 and 1 permil (fig. 19A). Inter-section variability in $\delta^{18}O_{carb}$, however, is much larger, and on the order of 5 to 6 permil (fig. 19B). Canyon-shoulder sections also exhibit strong covariation between $\delta^{13}C_{carb}$ and $\delta^{18}O_{carb}$, especially for sections 1–9 (r^2 values between 0.44 and 0.88; figs. 13B and 13D). Thus, regardless of the process driving the $\delta^{13}C_{carb}$ excursion, it is happening consistently and uniformly across the ARC.

In order to assess the provenance and relative timing of acquisition of $\delta^{13}C_{carb}$ and $\delta^{18}O_{carb}$ values in Wonoka carbonates, we performed an isotope conglomerate test on the breccia units of Mount Thomas, Oodnapanicken, and Saint Ronan canyon-fill (figs. 9, 11, and 12, respectively). Potential sources for the limestone and dolomite clasts of the breccia units include (a) eroded units from the canyon-shoulder (figs. 4 and 5) and (b) crust carbonates (fig. 15), especially for canyon-fill localities where in-place crust carbonate also is observed (such as Mount Thomas; fig. 9A). Isotopically, the crusts overlap with canyon-shoulder horizons and clasts; crust samples show very negative and variable $\delta^{13}C_{carb}$ values (the observed range is −10.3 to 1.5‰) and strong covariation with $\delta^{18}O_{carb}$ ($r^2 = 0.60$). The trace element dataset, however, shows that crust samples are geochemically distinct from both canyon-shoulder and clast carbonates (see *Trace Element Abundances* section). Specifically, crust samples show elevated metal abundances, especially for Al, Mn, K, Na, and Li (fig. 16). Crust [Mg] patterns are also distinct, showing intermediate Mg:Ca values not observed in canyon-shoulder or clast populations. Projections onto PC 1, which are weighted averages of trace element abundance (fig. 18D), corroborate these patterns seen in the individual

cross-plots of figure 16; crust samples have the highest PC 1 scores, and plot as a group distinct from other Wonoka carbonate samples.

Thus, high metal abundances of these carbonates (figs. 16 and 18D), relative to canyon-shoulder and clast carbonates, imply a different formation fluid for the crusts [or dramatically different precipitation kinetics; for example, Lorens (1981)]. Its stratigraphic relationship to the paleocanyon surface (that is, blanketing the canyon-wall, and striking at significant angle to the underlying Brachina Fm. and overlying Wonoka canyon-fill sediments; fig. 9A) suggests the crust precipitated *in-situ* (Eickhoff and others, 1988; Giddings and others, 2010). Eickhoff and others (1988), noting extreme isotopic depletion in $\delta^{13}C_{carb}$ and $\delta^{18}O_{carb}$, invoked subaerial exposure and subsequent tufa formation as a model for crust formation. Authigenic, submarine carbonates associated with hydrocarbon seeps, however, often have very negative $\delta^{13}C_{carb}$ values [for example, Aharon (1994); Haggerty (1991); Aharon and others (1997); Campbell and others (2002)]. Hydrocarbon-bearing fluids, generated within the sedimentary prism or contributed from greater depths, flow upwards towards the seafloor along preferred flow pathways. If oxidized via anoxic metabolisms at or near the sediment-water interface, hydrocarbon remineralization by microbial consortiums leads to a production of alkalinity and DIC, and therefore encourages $CaCO_3$ precipitation. The resulting precipitates appear as lenses or pods of micrite, isopachous cements and spar in dominantly siliciclastic successions (Campbell and others, 2002). The $\delta^{13}C_{carb}$ values of these precipitates can be extremely negative (between −50 and −40‰, if the hydrocarbons are thermogenic or biogenic methane); however, a huge range exists for Phanerozoic seep deposits (−50 to +15‰), depending on hydrocarbon composition (methane, oil fractions, sedimentary organic matter) and degree of mixing between pore fluids and contemporaneous DIC (Campbell and others, 2002). Importantly, seep carbonates display elevated abundances of certain trace metals (for example, [Fe], [Mn], [Al] and [Mg]), along with drops in [Sr], relative to contemporaneous $CaCO_3$ precipitated from seawater (Campbell and others, 2002). Therefore, authigenic carbonate formation associated with a hydrocarbon seep or oxidation of sedimentary organic matter is a model consistent with the geochemical and physical stratigraphic observations of crust carbonate (fig. 15).

Regardless of its origin, crust carbonate, based on its trace element geochemistry (figs. 16 and 18), does not appear to be an important component of the clast populations of Mount Thomas (fig. 9), Oodnapanicken (fig. 11) and Saint Ronan (fig. 12). Canyon-fill breccias, therefore, are primarily composed of eroded canyon-shoulder carbonates. If the clasts acquired their $\delta^{13}C_{carb}$ and $\delta^{18}O_{carb}$ values *in-situ* on the canyon-shoulders, then the breccia $\delta^{13}C_{carb}$ distribution should display the same isotopic range as the now-eroded canyon-shoulder. In contrast, if either the canyon-shoulder or the canyon-fill breccia units experienced post-depositional isotopic alteration, then the isotopic distributions of both populations could be disconnected. In this scenario, clasts from individual breccia beds may either (a) reflect the primary isotopic values in the shoulder (that is, not extremely depleted in $\delta^{13}C_{carb}$), or (b) hold consistent diagenetic values homogeneous within breccia units. Individual breccia units record substantial $\delta^{13}C_{carb}$ variability [the absolute ranges (maximum – minimum value) of $\delta^{13}C_{carb}$ are between 6 and 17‰] as well as significant linear correlation between $\delta^{13}C_{carb}$ and $\delta^{18}O_{carb}$ (figs. 10, 11, 12 and 14). These findings constitute a *positive* isotope conglomerate test, and require that both the negative $\delta^{13}C_{carb}$ values and the $\delta^{13}C$-$\delta^{18}O$ covariation were acquired in Wonoka Fm. canyon-shoulder carbonates *before* those carbonates were eroded and transported into the paleocanyons.

As all 12 measured sections represent complete samplings of the full Wonka thickness at similar 1 to 2 m resolution, the compiled relative distribution of $\delta^{13}C_{carb}$ values are stratigraphically-weighted. Therefore, the canyon-shoulder $\delta^{13}C_{carb}$ distri-

bution (fig. 14D) can be meaningfully compared to the $\delta^{13}C_{carb}$ spectra of the canyon-fill breccia units (figs. 14E-14G), which should represent discrete sampling of the canyon-shoulder. Despite matching $\delta^{13}C_{carb}$ values and variability, differences exist between canyon-shoulder horizons and breccia units in their isotopic distributions. For example, Mount Thomas breccias (figs. 9, 14A and 14E), whose isotopic ranges best match those of units 1–9 in the canyon-shoulder (figs. 13B and 14D), have a greater abundance of dolomites compared to the canyon-shoulder. This observation can be explained partly by sampling bias; for Mount Thomas breccias, 25 percent of the clasts collected for isotope conglomerate tests (figs. 10 and 14A) are dolomites, whereas the actual abundance of dolomites in breccia units, as measured by clast counts, is 12 percent. The clast count fraction is much closer to the abundance of dolomites in the compiled canyon-shoulder dataset (9%). Over-sampling of dolomites, however, can not explain the expanded $\delta^{13}C_{carb}$ *range* observed in the clast dolomites (figs. 14A and 14E); most canyon-shoulder dolomites are restricted to values above 0 permil (fig. 14D), whereas clast dolomites are found with $\delta^{13}C_{carb}$ ranging from −10 to 5 permil (fig. 14A).

A more subtle difference between Mount Thomas clast populations and canyon-shoulder horizons is in the relative frequencies of observed $\delta^{13}C_{carb}$ values. With clasts (fig. 14E), there is a surplus of values between −9 and −8 permil and a dearth of values between between −7 and −5 permil, when compared to the canyon-shoulder (fig. 14D). This observation can be explained either by (a) uneven sampling of the canyon-shoulder by breccia units or (b) some degree of diagenesis of canyon-shoulder localities before erosion and deposition into paleocanyons. The diagenesis required would be on the order of 1 to 2 permil in $\delta^{13}C_{carb}$ and preferentially would affect canyon-shoulder horizons with values between −7 and −5 permil (that is, between 150 and 600 m on the canyon-shoulder). If such affected canyon-shoulder localities were then eroded and redeposited as breccias, then this signal would not be preserved in the canyon-shoulder dataset (fig. 14E). More pervasive dolomitization in these now-eroded sections (which may have made them more susceptible to erosion) would also help explain the discrepancies in dolomite $\delta^{13}C_{carb}$ distributions.

Conclusively assigning a process to explain these differences in $\delta^{13}C_{carb}$ distributions is not possible with the current dataset. These differences, however, are *minor* in scale relative to the signal from the isotope conglomerate tests. Namely, 1 to 2 permil offsets in $\delta^{13}C_{carb}$ exist between clasts and canyon-shoulders, but this offset is relative to a 17 permil range that must have been present in clasts before those carbonates were brecciated and redeposited in the paleocanyons. As preserved carbonate crusts look different geochemically from clasts (figs. 16 and 18D), canyon-shoulder horizons are the most likely source for breccia units. Furthermore, these concerns (that is, the importance of the crusts, an overabundance of dolomite, a surplus of −9 to −8‰ $\delta^{13}C_{carb}$ values) are not applicable to all paleocanyon sites. The more proximal Saint Ronan canyon-fill appears to have captured a smaller portion of the eroded canyon-shoulder, and therefore exhibit a smaller $\delta^{13}C_{carb}$ range than the Mount Thomas breccias. Saint Ronan clasts, however, match the isotopic range and relative distribution, color and lithologies observed in units 3–8 of the immediately adjacent canyon-shoulder (measured sections 8-10 on figs. 5, 12A, and 14G).

Implications for Paleocanyon Formation

While differing models exist which seek to explain the formation of the Wonoka canyons—namely, subaerial (Christie-Blick and others, 1995) versus submarine (Giddings and others, 2010) mechanisms—there has been broad agreement that canyon incision occurred early during Wonoka Fm. deposition. Outcrop expression of canyon incision on the canyon-shoulder has been described as a cryptic unconformity, placed variably within Haines' units 1–5 [Christie-Blick and others (1995); Giddings and

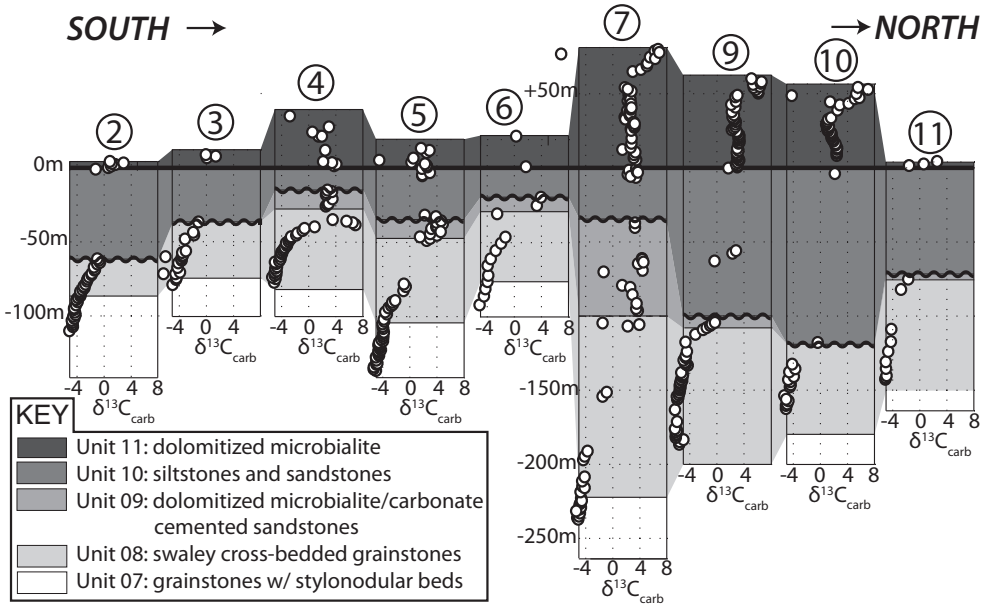

Fig. 20. Fence diagram of the upper units (7-11) of Wonoka canyon-shoulder sections. The diagram is hung from the base of unit 11 as a datum. Thicknesses of units 10 and 11 generally increase northwards. Values of $\delta^{13}C_{carb}$ at the base of unit 10 are generally positive, but the absolute value of the profile at this surface varies substantially from section-to-section (0 to +7‰). This variability is mainly controlled by the presence or absence of unit 9. Sections with a thinner or missing unit 9 often have a thicker unit 10, thus supporting erosive removal of unit 9 and transport and re-deposition into paleocanyons further north (figs. 3, 9, 11 and 12).

others (2010); figs. 4 and 5]. Given the presence of carbonate clasts with positive $\delta^{13}C_{carb}$ values in canyon-fill breccia units (figs. 14A and 14B), Husson and others (2012) proposed a higher surface (that is, above unit 8) to be responsible for at least some (but not necessarily all) of the canyon cutting at Mount Thomas and Oodnapanicken. Husson and others (2012) therefore placed a sequence boundary at the abrupt appearance of unit 10 siliciclastics, where the $\delta^{13}C_{carb}$ profile first recovers to positive $\delta^{13}C_{carb}$ values (fig. 13B). The more comprehensive physical and chemostratigraphic dataset presented in this work corroborates and strengthens this argument. Unit 9 is variably absent (that is, measured sections 2, 3, 8, 10 on figs. 4, 5 and 20) under this surface. Sections with a thicker, more complete unit 10 often also have a thinner, truncated unit 9, thus providing evidence that the surface is erosive (fig. 20). Thus, the canyon-fill sampled units 1–9 of intact canyon-shoulder stratigraphy, whose carbon isotopic range (−12 to +5‰) matches that of the tabular-clast breccias (figs. 9 and 11).

Above the basal breccias, the canyons are filled with the fine grained, wavy-laminated carbonate beds (fig. 13A) which represent a recycled and homogenized canyon-shoulder section, producing $\delta^{13}C_{carb}$ profiles (measured sections 13-15 in fig. 13A) that are stratigraphic averages of units 1–9 (fig. 14D). Statistics from the compiled canyon-shoulder (fig. 14D) and fine-grained canyon-fill (fig. 13A) datasets support this model. The mean $\delta^{13}C_{carb}$ value of the fine-grained canyon-fill sediments is −7.4 permil, ($1\sigma = 0.7$) compared to a mean value from canyon-shoulder units 1–9 of −6.8 permil ($1\sigma = 2.1$). Thus, the mean isotopic values of the canyon-shoulder and fine–grained canyon-fill datasets overlap, with the variance of the canyon-fill being

much smaller. This result is expected, as mixing and homogenization of a canyon-shoulder profile at a scale below that sampled for isotopic measurement should decrease the variance but produce a similar mean; where canyon-fill is not well mixed at the scale of isotopic measurement (that is, breccia clasts), the variance of the distribution is much larger (fig. 14E). These results are consistent with the model that the fine-grained, carbonate mudstones of Mount Thomas, Oodnapanicken, and Mount Goddard paleocanyons (sections 13-15 on fig. 13A) represent recycled, ground-up and redeposited canyon-shoulder units 1–9.

We do not claim that the proposed surface at the base of unit 10 represents all canyon cut-fill sequences within the Wonoka Fm., as workers have documented numerous intervals of canyon incision throughout Wonoka Fm. deposition (DiBona and von der Borch, 1993). For example, the Saint Ronan paleocanyon is immediately adjacent to well-developed canyon-shoulder successions (measured sections 8-10 on figs. 5 and 12A), making these sections good targets to search for potentially subtler expressions of canyon-cutting on the intact canyon-shoulder. The most positive $\delta^{13}C_{carb}$ value observed from the Saint Ronan breccias is −2.5 permil, corresponding isotopically to unit 8 of measured sections 8–10 on (fig. 5). In these sections, the unit 3/4 contact is an abrupt transition from red to green silt interbeds (fig. 6D) and marked by tabular-intraclast breccia (fig. 6E). In section 9, unit 3 is 150 m of red siltstones interbedded with thin-bedded (2-5 cm) wavy laminated carbonate beds; in section 10, unit 3 is 10 m thick (fig. 12A). The unit 3/4 contact is also a major transition in $\delta^{13}C_{carb}$ profile; unit 3 carbonates show a smooth recovery from −12 to −7.5 permil, whereas unit 4 is the base of 300 to 400 m of invariant $\delta^{13}C_{carb}$ values (figs. 4, 5 and 13B). If the $\delta^{13}C_{carb}$ excursion preserved in the Wonoka Fm. does record a global, secular isotopic change in DIC, sedimentation rates for this 300 to 400 m portion of Wonoka stratigraphy would be required to be the fastest relative to other Ediacaran basins (fig. 1C). Fast sedimentation rates would make the lower Wonoka more prone to depositional oversteepening and slope failure on the upper slope, thus triggering downslope sediment flows that erode preexisting bathymetric lows and establish the beginnings of submarine canyon channels (Pratson and Coakley, 1996).

These observations suggest that a paleocanyon surface at Saint Ronan emanated from the unit 3/4 contact (Haines, ms, 1987). At Saint Ronan, canyon-cutting eroded at least 150 m of lower Wonoka carbonates and siltstones. Basal canyon-fill is composed of 0.1 to 0.9 m thick tabular-clast breccias interbedded with green siltstone and unconformably overlies the red siltstones and sandstones of the Bunyeroo Fm. (fig. 12B). The Saint Ronan canyon must have (a) remained open to sediment in-fill throughout the deposition of unit 7 on the canyon-shoulder to fully explain the $\delta^{13}C_{carb}$ range observed in the Saint Ronan breccias and (b) been closed by the time of unit 10 and 11 deposition, as both units blanket the canyon-fill stratigraphy (fig. 12A). This observation requires that canyon formation occurred during ongoing Wonoka sedimentation, and therefore demands a syn-depositional age for the low $\delta^{13}C_{carb}$ values of the canyon breccia clasts and associated shoulder stratigraphy.

Explaining Basin Scale Chemostratigraphic Trends

While Wonoka Fm. canyon shoulders preserve a deeply negative $\delta^{13}C_{carb}$ excursion (−12 to +5‰) with remarkable consistency across the ARC (figs. 4, 5 and 13B) and isotope conglomerate tests require acquisition of the excursion before those carbonates were brecciated and redeposited in the paleocanyons (fig. 14), the excursion signal differs slightly and subtly across the basin. Between canyon-shoulder sections, $\delta^{13}C_{carb}$ profiles differ by ~0.5 to 1 permil (expressed as $\Delta^{13}C$, or the difference between an individual section and the basin-averaged $\delta^{13}C_{carb}$ profile; fig. 13B). These differences are geographically organized, with more southerly sections being more negative in $\Delta^{13}C$ than more northerly sections (fig. 19A). Differences in

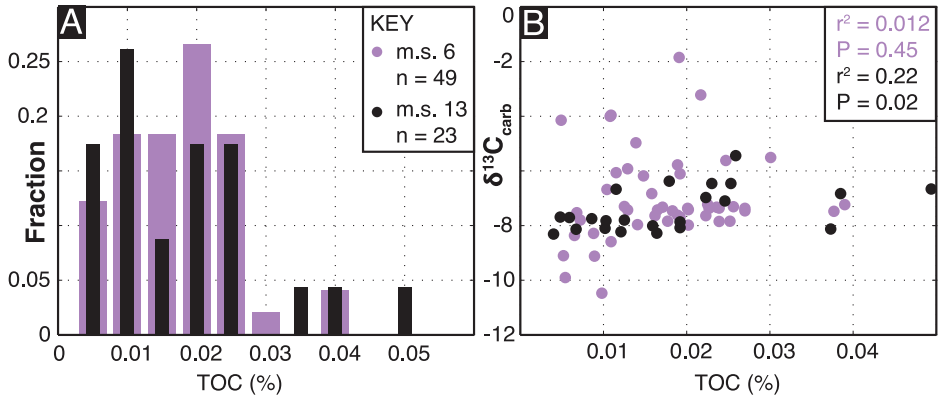

Fig. 21. Total organic carbon contents from two localities (a canyon-shoulder (6) and canyonfill (13) section). (A) The relative frequency and range of TOC values for sediments from these two localities overlap, and (B) no relationship with coeval $\delta^{13}C_{carb}$ measured from the same sample is apparent.

$\delta^{13}C_{carb}$ ($\Delta^{18}O$) are much larger, but lack geographic structure (fig. 19B). In the modern ocean, 1 to 1.5 permil gradients in $\delta^{13}C$ of DIC are driven by the biological pump, with primary production and export of organic matter enriching ocean water masses in ^{13}C (Kroopnick, 1985). Thus, the differences in $\delta^{13}C_{carb}$ profiles across the ARC could be a primary lateral gradient in $\delta^{13}C_{carb}$, and would imply more productive (and ^{13}C enriched) waters in the northern ARC. Such a gradient is consistent with a northern basin-deepening trend, seen in facies relationships in the Wonoka (that is, siltier, thicker, and finer grained in the more northern sections; figs. 4, 5, and 20) and in the Nuccaleena Fm. (Rose and Maloof, 2010). However, differences in total organic carbon (TOC) abundances between a southern and northern locality (measured section 6 (canyon-shoulder) and 13 (canyon-fill), respectively; fig. 3A) are not resolvable (fig. 21A). This observation implies (a) that no lateral gradient in primary productivity existed, (b) that measured sections 6 and 13 are too close spatially to resolve such a gradient, or (c) that Wonoka TOC values are not faithful recorders of primary organic carbon content of Wonoka sediments.

Conversely, the offsets could be the result of differential diagenesis between sections, with more southerly sections recording small-scale ($< 1‰$) shifts in $\delta^{13}C_{carb}$ resulting from interactions with ^{13}C-depleted diagenetic fluids. This model finds support in the physical stratigraphic record, as more southerly sections have a greater abundance of stylondular bedding (fig. 19A), a putatively diagenetic texture [Haines (1988); fig. 7)] that does result in negative shifts in $\delta^{13}C_{carb}$ (fig. 17A). This relationship can be quantified, as there exists a correlation between the amount of $\delta^{13}C_{carb}$ offset found in a given section (expressed as median $\Delta^{13}C$) and the section abundance of stylonodular bedding (fig. 19C). Thus, sections with more physical evidence of diagenetic alteration also have more negative values in $\Delta^{13}C$, and suggest that differences in $\Delta^{13}C$ are the result of small-scale diagenesis.

Despite this correlation, an explicit causal connection between stylondular bed formation and this basin-wide $\delta^{13}C_{carb}$ gradient is not immediately apparent. While the observed $\delta^{13}C_{carb}$ offsets caused by this sedimentary diagenesis (fig. 17) are at the same scale isotopically as differences in median $\Delta^{13}C$ values (fig. 19A), stylonodular bed formation, where present, is restricted to ~50 to 200 m of upper Wonoka stratigraphy (figs. 4 and 5); by thickness, the maximum abundance of stylonodular beds in a measured section is 5.8 permil. Thus, it is not clear how relatively small amounts of diagenetically altered carbonate can offset the $\delta^{13}C_{carb}$ profiles recorded in ~700 m of

mostly well-preserved (figs. 6B-6F) canyon-shoulder carbonate. Observed correlations between the strength of $\delta^{13}C_{carb}$-$\delta^{18}O_{carb}$ covariation (expressed as r^2 values of the different canyon-shoulder section datasets) and (i) median $\Delta^{13}C$ (fig. 19D) and (ii) stylonodular bedding abundance (fig. 19E) are even more puzzling. Median $\Delta^{13}C$ differences (fig. 19A) and diagenetic $\delta^{13}C_{carb}$ offsets from nodule formation (fig. 17A) are on similar <1 permil scale, whereas correlations between the $\delta^{13}C_{carb}$ and $\delta^{18}O_{carb}$ of canyon-shoulder carbonates occurs over 5 and 10 permil of isotopic variability expressed in 100s of meters of canyon-shoulder stratigraphy. How the three are related mechanistically (figs. 19D and 19E) is not obvious, nor is identifying causal relationships and driving variables within any of these correlations.

Most likely, these correlations are indicative of an *environment*, either sedimentary or diagenetic in character, which is amenable to stylonodular bed formation, ~0.5 to 1 permil offsets in $\Delta^{13}C$, and better preservation of $\delta^{13}C_{carb}$-$\delta^{18}O_{carb}$ covariation. For example, the Wonoka Fm. thickens and deepens northward (~600 m in the south, and ~850 m in the north; figs. 4 and 5); if its base and top are time-equivalent, as is suggested by the observed $\delta^{13}C_{carb}$ profile across the basin (fig. 13B), then this observation necessitates slower, time-averaged sedimentation rates in the south. Longer hiatuses in more southerly sections (that is, longer time intervals between event beds) would decrease the long-term sedimentation rate. Given that much of the Wonoka Fm. (in both the north and south) is composed of discrete, rapidly-deposited event beds (figs. 6F-6H), longer hiatuses seem a more likely explanation than a constant, northwardly increasing sedimentation rate. Longer hiatuses may also allow for the more frequent development of stylonodular beds and for thicker stylonodular diffusive fronts to develop. Evidence for this relationship is seen in the stratigraphic dataset (figs. 4 and 5); the median thickness of stylonodular beds in measured section 1 (fig. 4; nodular bed abundance of 5.8%) is 0.8 m, whereas in measured section 10 (fig 5; nodular bed abundance of 0.3%), the median thickness is 0.25 m. Longer hiatuses also may result in larger negative $\delta^{13}C$ offsets in these more southerly sections (figs. 19A and 19C), a result of both (a) the thicker stylonodular beds and (b) longer time of contact between deposited sediments and putatively $\delta^{13}C$-depleted bottom waters (fig. 17B), thereby allowing more opportunity for recrystallization and isotopic resetting.

Testing Hypotheses for the Origin of the "Shuram" Excursion in South Australia

Taken together, these stratigraphic and isotopic observations preclude burial diagenesis models for the negative isotopic values in South Australia [Derry (2010); fig. 2C]. The low $\delta^{13}C_{carb}$ values and $\delta^{13}C$-$\delta^{18}O$ covariation of the Wonoka Fm. must either be primary or a relatively early diagenetic signal (that is, before theWonoka canyons began to fill, and certainly prior to burial). Both meteoric diagenesis (Knauth and Kennedy, 2009) and authigenic carbonate formation (Schrag and others, 2013) are examples of early alteration. For the authigenic model (fig. 2D), the physical stratigraphy of the Wonoka Fm. does not provide first order support. The authigenic model requires the early in-growth of carbonate in the sediment column, and such carbonates appear as crystal fans, voidfilling cements, and secondary nodules in the rock record (Grotzinger and James, 2000). Wonoka carbonates, however, show excellent preservation of primary sedimentary bedforms (figs. 6E-6I). Wonoka carbonates did *not* form in-place—they record mobilization and deposition of carbonate grains via a range of sedimentary processes—with two exceptions. The first is stylonodular bedding (fig. 7), which does record an authigenic process of dissolution and reprecipitation. The carbon isotope effect of this process, however, is a negative shift of only 0.3 to 0.4 permil, and thus cannot be used to explain the full 17 permil excursion signal observed across the basin.

The second are the crusts (fig. 15), which formed on paleocanyon surfaces at Mount Thomas (fig. 9A). The isotope conglomerate tests, however, require canyon-

filling to have occurred after deposition of canyon-shoulder units 1–9 to explain the 17 permil variability seen in breccia units (figs. 14A and 14E). The canyon-shoulder $\delta^{13}C_{carb}$ profile had therefore already recovered to positive values before carbonate crusts formed. If the canyons were cut earlier than the unit 9/10 boundary, and remained unfilled through Wonoka canyon-shoulder deposition, then carbonate crust formation could have occurred throughout canyon-shoulder deposition; breccia formation and canyon-filling would then have been synchronous with terminal Wonoka deposition, after canyon-shoulder horizons with positive $\delta^{13}C_{carb}$ were available for erosion. Differences in trace element geochemistry (figs. 16 and 18D), however, still make it unlikely that carbonate crust and canyon-shoulder were formed from similar fluids, and are therefore not recording the same carbon isotope signal. Thus, to apply the authigenic model to the observations from South Australia, a location of authigenic carbonate production must act as a source for Wonoka sedimentation. This carbonate must first be produced at (or near) the sediment-water interface somewhere in the basin. Authigenic carbonate must then be mobilized and re-deposited as sedimentary beds, with comparable admixtures between authigenic and marine carbonate grains produced homogeneously across the basin to record the consistent 17 permil signal seen in the canyon-shoulders sections (fig. 13B).

The geological evidence from South Australia similarly does not support the meteoric model (fig. 2B). In classic examples of meteoric diagenesis, $\delta^{13}C_{carb}$ values are most negative beneath exposure surfaces (fig. 2B), a result of top-down infiltration and recrystallization by the altering fluid [for example, rainwater carrying isotopically light DIC as a result of soil respiration (Allan and Matthews, 1982; Melim and others, 2001)]. In the Wonoka Fm., the only physical evidence for subaerial exposure is at the top. Mudcracks are locally observed in unit 10 sandstones (Haines, ms, 1987) and fenestral carbonate fabrics are found in the dolomitized microbialites of unit 11. At Saint Ronan, however, both of these units are developed at the top of both canyon-shoulder and canyon-fill sections, thus indicating that the canyons were cut and filled before unit 11 deposition (fig. 12A). Canyon-shoulder horizons, eroded to breccia clasts, had therefore already acquired negative $\delta^{13}C_{carb}$ values before subaerial exposure of units 10 and 11. If such exposure resulted in isotopic alteration, it cannot be invoked to explain the $\delta^{13}C_{carb}$ values of either units 1–9 or the breccia populations.

Although our proposed sequence boundaries at the bases of units 4 and 10 could be submarine, following the canyon-formation models of Pratson and Coakley (1996) and Giddings and others (2010), some have argued that the Wonoka canyons formed as result of a Messinian-style salinity crisis, with the base level fall and subaerial exposure of the Wonoka Fm. accomplished by basin isolation (Christie-Blick and others, 1990). This scenario would leave the canyon-shoulders as much as 1.5 km above local sea level and therefore susceptible to meteoric diagenesis. However, based on the isotope conglomerate tests (figs. 14A-14C), in this scenario, diagenesis would need to occur *after* the Wonoka Fm. was exposed but *before* any substantial canyon cutting and redeposition of shoulder rocks into canyon-fill had occurred. Although our data do not rule out this possibility explicitly, there is no visible evidence of such alteration in the form of widespread recrystallization, karstic surfaces or dissolution collapse breccias at the unit 9/10 contact (or anywhere within the Wonoka Fm.). Primary sedimentary fabrics are exceptionally well preserved in the Wonoka Fm. (figs. 6 and 8), and preserving the small diagenetic offsets resulting from nodular bed formation (0.3-0.4‰ on 5 cm scale; fig. 17) is inconsistent with large-scale isotopic modification. In fact, the coarsest recrystallization observed is in connection with dolomite growth in unit 11 (Husson and others, 2012), where $\delta^{13}C_{carb}$ values are at their most positive (+2 to +8‰; fig. 13B). Also, as the meteoric model hinges upon fluid-rock interactions, the lightest isotopic values should be found in the most permeable strata within the

Wonoka Fm. Permeability—a function of grain size, shape and packing—is thus directly related to lithofacies, and contrary to these predictions, there is no obvious pattern of facies-dependent isotope sorting (fig. 13E). Furthermore, the $\delta^{13}C_{carb}$ profile of the canyon-shoulders (most negative at the bottom and increasing upwards) is opposite in pattern from first-order predictions of top-down alteration emanating from an exposure surface (Allan and Matthews, 1982). Lastly, Messinian-style isolation and meteoric diagenesis would be a local event, restricted in space to South Australia, and would not explain the strata-bound nature of the negative carbon isotope values of other Ediacaran basins (even if the excursions are not truly synchronous; fig. 1).

Implications for Global Models of the "Shuram" Excursion

Field and geochemical observations require a syn-depositional age for the $\delta^{13}C_{carb}$ excursion observed in the Wonoka Fm. Therefore, possible explanatory models are that the signal is (a) a record of secular change in global DIC (Rothman and others, 2003; Fike and others, 2006; Bjerrum and Canfield, 2011), (b) a record of local change, specific to ARC waters, or (c) a result of subtle, syn-depositional sedimentary diagenesis which overprints primary $\delta^{13}C_{carb}$ values but preserves primary sedimentary fabrics and the very early diagenetic textures and geochemical signals of stylonodular beds (see *Geochemistry of Stylonodular Beds* section; figs. 7 and 17). Rather than choosing a single model as the most likely, this final section evaluates each of these different models, and explicitly articulates the demands and constraints that *any* model must satisfy to explain the Wonoka dataset.

Absolute ages of sedimentary successions hosting the "Shuram" excursion are the true tests for global models, as such constraints would simultaneously evaluate global synchroneity of "Shuram" excursions (Grotzinger and others, 2011) as well as rigorously quantify the fluxes of $\delta^{13}C$-depleted carbon required to drive the excursion. For example, in the model of Bristow and Kennedy (2008), an injection of 384,000 gigatons (Gt) of light carbon ($\delta^{13}C = -30‰$) was needed to drive an excursion lasting 1.3 Myr. Such a pulse would be ~75× larger than modeled injections needed to drive the Paleocene-Eocene Thermal Maximum (PETM) $\delta^{13}C$ excursion (Higgins and Schrag, 2006), which warmed the deep ocean by 4–5 °C (Kennett and Stott, 1991) and shoaled the carbonate compensation depth of the deep ocean by ~2 km (Zachos and others, 2005). In certain ways, the stratigraphic expression of the "Shuram" excursion is similar to the PETM. Compared to the recovery, the "Shuram" $\delta^{13}C_{carb}$ downturn is poorly preserved, hosted in very thin (or even non-existent, as in South Australia) intervals composed of relatively few carbonate beds (fig. 1A). This pattern is suggestive of waters initially corrosive to $CaCO_3$ deposition, followed by recovery of carbonate deposition as silicate weathering consumes the injected carbon and supplies an overabundance (that is, above Ediacaran background fluxes) of alkalinity to the world's oceans (Zachos and others, 2005).

Such a scenario would make Shuram recovery carbonates akin to post-glacial "cap-carbonate" sequences that blanket the "snowball Earth" glacial deposits of the Neoproterozoic [Hoffman and others (1998); although the Wonoka Fm. is not a transgressive systems tract], and would help explain the preservation of Ediacaran carbonates in basins otherwise dominated by siliciclastics, such as in South Australia, where the Nuccaleena (1 to 30 m thick) and Wonoka (~700 m) formations are the only carbonate units in the 3 to 5 km thick Wilpena Group (Preiss, 2000). The viability of such a model is highly dependent upon the duration of the Shuram excursion. Even if such a large pool of depleted carbon were available for remineralization, perhaps present as the "big DOC" pool as described in Rothman and others (2003), the oxidant budget of the modern ocean would be exhausted if the excursion lasted more than 2.5 Myr (Bristow and Kennedy, 2008). While it is commonly assumed the duration must have been muilt-million year in scale because Shuram-like excursions are preserved in

100s of meters of sediment (fig. 1A), a duration of 1 Myr would yield very high, but not unreasonable, sedimentation rates. For instance, in the Wonoka Fm., a thick succession compared to other Ediacaran examples (fig. 1), sedimentation rates would be ~0.5 to 0.6 m/kyr, which are on the high end of long-term average sedimentation rates seen in global compilations (Sadler, 1981; Peters, 2006) and ~10× higher than average sedimentation rates measured in sediment cores of modern periplatform carbonate sediments (Eberli and others, 2002).

The interpretation of the $\delta^{13}C_{carb}$ excursion observed in the Wonoka Fm. as a record of local water column processes was developed originally by Calver (2000), who contended that the extremely depleted $\delta^{13}C_{carb}$ values observed were a product of a salinity-stratified basin with limited open marine connections. The model posits that Wonoka carbonates acquired their $\delta^{13}C_{carb}$ values from bottom waters, thus requiring a ~15 permil depth gradient in $\delta^{13}C_{DIC}$ for ARC waters. Such a gradient would dwarf the ~1–2 permil depth gradients of the modern ocean (Kroopnick, 1985) and would be twice as large as in the Black Sea (Fry and others, 1991), but is equal to isotopic differentiation observed in some modern meromictic lakes (Deevey and others, 1963). Extreme isotopic depletion (down to −9‰) also has been observed in local surface DIC of isolated brines (Lazar and Erez, 1992), wherein intense photosynthetic activity can deplete DIC concentrations to 50 percent of levels predicted from equilibrium with the atmosphere. This disequilibrium is maintained dynamically, and leads to an invasion of isotopically-light CO_2. A common requirement for both models would be a vigorous biological pump, at least locally, to maintain either the 15 permil depth gradient or surface CO_2 disequilibrium. As with the meteoric hypothesis, these "local-water column" hypotheses would be restricted to a silled and isolated ARC. It is not obvious how such a mechanism could explain similar levels of isotopic depletion observed in other Ediacaran basins (fig. 1), nor why such extreme depletion in sedimentary carbonates are restricted broadly to the Ediacaran Period (Grotzinger and others, 2011).

A universal phenomena observed in modern neritic carbonates, which are predominately biogenic aragonite and high-Mg calcite, is their syn-depositional recrystallization to more thermodynamically stable crystallites. This recrystallization is documented by textural evidence (Macintyre and Reid, 1995; Furukawa and others, 1997; Reid and Macintyre, 1998) as well as down-core changes in pore water geochemistry (Walter and others, 2007), and is driven strongly by the excess surface free energy derived from the very small crystal sizes of biogenic grains (Walter and Morse, 1984). A study of the isotopic effect of this early neomorphism in the Florida Keys has shown little change in the $\delta^{13}C$ of the bulk carbonate sediment (Walter and others, 2007), suggesting that in modern environments, the isotopic effect is not large. However, if syn-depositional recrystallization from meta-stable to stable crystal forms was prevalent in Ediacaran shallow-water carbonates [namely, if the primary $CaCO_3$ polymorph was aragonite, as is predicted in some models of Ediacaran seawater chemistry; Lowenstein and others (2001)], it is important to consider possible isotopic effects in an Earth surface system with putatively very different boundary conditions. For example, if O_2 and SO_4^{2-} concentrations in Ediacaran oceans were low enough, sulfate reduction, and concomitant anaerobic oxidation of methane (AOM), can occur just below the sediment-water interface, and perhaps overlap with the zone of syn-sedimentary recrystallization [though oxidant levels were probably not too low if the Wonoka Fm. is ~ 560 Ma (Bowring and others, 2007) and thus significantly post-dates the rise and establishment of the Ediacaran Biota (Bowring and others, 2003)]. The resultant $\delta^{13}C$ of the neomorphosed $CaCO_3$ would be a balance of isotopic inputs from the dissolved $CaCO_3$, diffused seawater DIC from above, and the remineralized methane ($\delta^{13}C$ ~ −60‰).

Thus, the depleted $\delta^{13}C_{carb}$ values of the Wonoka Fm. could be a result of syn-depositional, fabric-retentive recrystallization and shallow AOM. The degree of recrystallization is required to be extremely consistent across the ARC, with progressively less and less incorporation of AOM-derived DIC into neomorphosed carbonate with time, to produce the basin-wide, smooth $\delta^{13}C_{carb}$ curve of −12 to +5 permil preserved in the Wonoka Fm. (fig. 13). Also, the driving force for this process would be organic carbon content (TOC) of Wonoka sediments, which are consistently low (0.01-0.05%, as measured in sections 6 and 13; fig. 21A) and show no relationship with $\delta^{13}C_{carb}$ (that is, lower $\delta^{13}C_{carb}$ with higher TOC values; 21B). These TOC values are low for modern platform carbonates [0.1-0.9%; Oehlert and others (2012)] and are extremely low for formations where authigenic carbonate formation is observed [for example, 2-5% for the Miocene Monterey Formation; Behl (1999)]. Thus, if AOM is to be invoked as a process important for Wonoka geochemistry, one must argue that TOC values were higher prior to lithification and isotopic modification, and have since been altered to lower values.

Lastly, isotopic modification by AOM must have occurred *before* stylonodular bed formation, as this fabric likely formed during hard ground formation (Haines, 1988) and the associated ~0.5 permil negative shift in $\delta^{13}C_{carb}$ is well-preserved in the Wonoka Fm. (figs. 17A and 19C). For example, if the $\delta^{13}C_{carb}$ excursion was 1 Myr in duration and hiatuses represent the majority of time recorded in the Wonoka Fm., then hard grounds which preserve stylonodular bedding lasted an average of ~2500 years, during which time AOM must act to alter the primary $\delta^{13}C$ of the carbonate bed before nodule formation begins. It should be stressed that this duration is a *maximum* estimate; hard grounds are likely preserved which do not host stylonodular bedding, nor is sedimentation between those hard grounds instantaneous. This exercise demonstrates, however, that the presence of stylonodular bedding, a product of syn-depositional recrystallization which only resulted in ~0.5 permil changes in $\delta^{13}C$, will be a useful constraint in future models of syn-depositional diagenesis in the Wonoka Fm. This model would be a variant of the authigenic model of Schrag and others (2013), which invoked AOM under low-O_2 boundary conditions to produce $\delta^{13}C$-depleted porewater DIC but contended that its record would be housed in texturally distinct cements and sea-floor precipitates. In this context, the extremely $\delta^{13}C$-depleted carbonates of the Ediacaran could represent syn-depositional diagenesis, and still reflect evolving redox conditions. The Ediacaran Period may represent an ideal time for this process to be recorded in the rock record; SO_4^{2-} levels could have been high enough to drive extensive AOM, but low enough such that the AOM zone is shallow in the sediment column.

As discussed above, radiometric ages would be best suited for testing these three different hypotheses. Even in the absence of absolute time, analyses of other isotopic tracers, especially those with modeled residence times that are orders-of-magnitude different from carbon, such as $\delta^{44/40}Ca$ and $\delta^{26}Mg$, are useful next steps towards understanding the "Shuram" excursion. Synchronous changes in the C, Ca and Mg isotopic systems are not predicted if the records represent long-term evolution of the global ocean. Searching for such changes would provide useful constraints on whether the geochemical signatures of the "Shuram" excursion are the result of changes in the global carbon reservoir, or local, early diagenetic expressions of a change in global boundary conditions (for example, O_2 and SO_4^{2-} concentrations). Each of these models has serious concerns to address with regards to the Wonoka and other Ediacaran carbonate datasets. For primary DIC models, the timescale, carbon injection requirements and oxidant budget demands must be better constrained. For local water-column processes, reasons for the 'Shuram' excursion's global and strata-bound development must be developed. For authigenic carbonate models, isotopic alteration

must be syndepositional, fabric-retentive, global, extremely consistent across a basin and important for strata that are presently low in TOC abundance.

CONCLUSIONS

Across the Adelaide Rift Complex, the Wonoka Formation hosts a deeply negative $\delta^{13}C_{carb}$ excursion (−12 to +5‰) with remarkable consistency across 12,000 km^2 of basin area. Fabric destructive diagenesis is variably present, only results in diagenetic $\delta^{13}C_{carb}$ offsets of < 1 permil, and can therefore not explain the isotopic variability observed in the Wonoka Formation. Trace element analysis fingerprints canyon-shoulder carbonates as the most likely source feeding the canyon-fill breccias of theWonoka paleocanyons. Therefore, based on the *isotope conglomerate tests*, Wonoka Formation canyon-shoulder sediments acquired the observed $\delta^{13}C_{carb}$ range (−12 to +5‰) before being eroded and transported as canyon-fill deposits. The surface responsible for the cut-fill sequences of the deepest paleocanyons sits high on the canyon-shoulder, and canyon-filling ceased before the development of the upper Wonoka Formation microbialitic reefs. These results are incompatible with a late-stage origin for the observed $\delta^{13}C_{carb}$ excursion in South Australia, and the first-order stratigraphic and microtextural patterns predicted by meteoric diagenesis and the authigenic model are not observed. Therefore, the balance of evidence supports either a primary origin or syn-depositional, fabric-retentive diagenesis for the extraordinary range of $\delta^{13}C_{carb}$ values seen in the Wonoka Formation of South Australia. Regardless, such extreme isotopic depletion in marine carbonate successions ($\delta^{13}C_{carb}$ values down to −12‰) are restricted in time to the terminal period of the Proterozoic Eon, and are products of Earth's surface environment. Therefore, adequate models must not only explain the geochemical and stratigraphic observations detailed above, but also explain why such excursions are unique to the Ediacaran Period.

ACKNOWLEDGMENTS

J.M.H was supported by the National Science Foundation Graduate Research Fellowship Program (NSF-GRFP), A.C.M. was supported by the Alfred Sloan Fellowship, A.C.M. and B.S. were supported by NSF grant EAR-1121034 to Maloof and Schoene, and Princeton University supported field and laboratory work. Blake Dyer, Laura Poppick, Brenhin Keller and Diogo Adrados provided assistance in the field. We thank Jim Gehling for fruitful discussions about Wonoka Formation stratigraphy. We thank the landowners and pastoralists of South Australia for land access. Rebecca Marks, Elizabeth Lundstrom, Jake Reznick, Steve Shonts, Jenny Piela, Mary Van Dyke, Cameron Webb, Simon Johansen, Natalie Saenz, Alison Campion, Nan Jiang, Collin Edwards, Leah Nelson, Katherine McLellan, and Josh Zoellmer helped with sample preparation. Stable isotope measurements were preformed at Princeton University by Laura Poppick with technical assistance from Sergey Olyenik and at the University of Michigan by Lora Wingate and Kacey Lohmann. Akshay Mehra helped draft figure 17. This manuscript was greatly improved by constructive reviews from Gordon Love, Magdalena Osburn and an anonymous reviewer.

Author Contributions

Following initial project planning by J.M.H. and A.C.M., field work was conducted by J.M.H. (4 field seasons), A.C.M. (2 field seasons), B.S. (1 field season) and C.Y.C. (1 field season). C.Y.C. worked on the Saint Ronan paleocanyon complex (fig. 12) as part of an undergraduate independent research project. J.A.H. supervised and advised J.M.H. with trace element abundance analytical work and data reduction. J.M.H. analyzed the data, wrote the manuscript and drafted figures, all with input from A.C.M., B.S., J.A.H., and C.Y.C.

References

Aharon, P., 1994, Geology and biology of modern and ancient submarine hydrocarbon seeps and vents: an introduction: Geo-Marine Letters, v. 14, n. 2–3, p. 69–73, http://dx.doi.org/10.1007/BF01203716

Aharon, P., Schwarcz, H. P., and Roberts, H. H., 1997, Radiometric dating of submarine hydrocarbon seeps in the Gulf of Mexico: Geological Society of America Bulletin, v. 109, n. 5, p. 568–579, http://dx.doi.org/10.1130/0016-7606(1997)109<0568:RDOSHS>2.3.CO;2

Allan, J. R., and Matthews, R. K., 1982, Isotope signatures associated with early meteoric diagenesis: Sedimentology, v. 29, n. 6, p. 797–817, http://dx.doi.org/10.1111/j.1365-3091.1982.tb00085.x

Baker, P. A., and Kastner, M., 1981, Constraints on the formation of sedimentary dolomite: Science, v. 213, n. 4504, p. 214–216, http://dx.doi.org/10.1126/science.213.4504.214

Banner, J. L., and Hanson, G. N., 1990, Calculation of simultaneous isotopic and trace element variations during water-rock interaction with applications to carbonate diagenesis: Geochimica et Cosmochimicha Acta, v. 54, n. 11, p. 3123–3137, http://dx.doi.org/10.1016/0016-7037(90)90128-8

Barnes, C. E., and Cochran, J. K., 1990, Uranium removal in oceanic sediments and the oceanic U balance: Earth and Planetary Science Letters, v. 97, n. 1–2, p. 94–101, http://dx.doi.org/10.1016/0012-821X(90)90101-3

Behl, R. J., 1999, Since bramlette (1946): The Miocene Monterey Formation of California revisited, *in* Moores, E. M., Sloan, D., and Stout, D. L., editors, Classic Cordilleran Concepts: A View from California: Geological Society of America, Special Paper, v. 338, p. 301–313, http://dx.doi.org/10.1130/0-8137-2338-8.301

Bergmann, K. D., Zentmyer, R. A., and Fischer, W. W., 2011, The stratigraphic expression of a large negative carbon isotope excursion from the Ediacaran Johnnie Formation, Death Valley: Precambrian Research, v. 188, n. 1–4, p. 45–56, http://dx.doi.org/10.1016/j.precamres.2011.03.014

Bjerrum, C. J., and Canfield, D. E., 2011, Towards a quantitative understanding of the late Neoproterozoic carbon cycle: Proceedings of the National Academy of Sciences of the United States of America, v. 108, n. 14, p. 5542–5547, http://dx.doi.org/10.1073/pnas.1101755108

Bowring, S., Myrow, P., Landing, E., Ramezani, J., Condon, D., and Hoffmann, K., 2003, Geochronological constaints on Neoproterozoic glaciations and the rise of Metazoans: Geological Society of America Abstracts with Programs, v. 35, n. 6, p. A516.

Bowring, S. A., Grotzinger, J. P., Condon, D. J., Ramezani, J., Newall, M. J., and Allen, P. A., 2007, Geochronologic constraints on the chronostratigraphic framework of the Neoproterozoic Huqf Supergroup, Sultanate of Oman: American Journal of Science, v. 307, n. 10, p. 1097–1145, http://dx.doi.org/10.2475/10.2007.01

Brain, C., Prave, A. R., Hoffmann, K.-H., Fallick, A. E., Botha, A., Herd, D. A., Sturrock, C., Young, I., Condon, D. J., and Allison, S. G., 2012, The first animals: *ca.* 760-million-year-old sponge-like fossils from Namibia: South African Journal of Science, v. 108, http://dx.doi.org/10.4102/sajs.v108i1/2.658

Bristow, T. F., and Kennedy, M. J., 2008, Carbon isotope excursions and the oxidant budget of the Ediacaran atmosphere and ocean: Geology, v. 36, n. 11, p. 863–866, http://dx.doi.org/10.1130/G24968A.1

Burns, S. J., and Matter, A., 1993, Carbon isotopic record of the latest Proterozoic from Oman: Eclogae Geologicae Helvetiae, v. 86, n. 2, p. 595–607.

Calver, C. R., 2000, Isotope stratigraphy of the Ediacaran (Neoproterozoic III) of the Adelaide Rift Complex, Australia, and the overprint of water column stratification: Precambrian Research, v. 100, n. 1–3, p. 121–150, http://dx.doi.org/10.1016/S0301-9268(99)00072-8

Calver, C. R., Crowley, J. L., Wingate, M. T. D., Evans, D. A. D., Raub, T. D., and Schmitz, M. D., 2013, Globally synchronous Marinoan deglaciation indicated by U-Pb geochronology of the Cottons Breccia, Tasmania, Australia: Geology, v. 41, n. 10, p. 1127–1130, http://dx.doi.org/10.1130/G34568.1

Campbell, K. A., Farmer, J. D., and Des Marais, D., 2002, Ancient hydrocarbon seeps from the Mesozoic convergent margin of California: carbonate geochemistry, fluids and palaeoenvironments: Geofluids, v. 2, n. 2, p. 63–94, http://dx.doi.org/10.1046/j.1468-8123.2002.00022.x

Canfield, D. E., Poulton, S. W., and Narbonne, G. M., 2007, Late-Neoproterozoic deep-ocean oxygenation and the rise of animal life: Science, v. 315, n. 5808, p. 92–95, http://dx.doi.org/10.1126/science.1135013

Christie-Blick, N., von der Borch, C. C., and DiBona, P. A., 1990, Working hypotheses for the origin of the Wonoka canyons (Neoproterozoic), South Australia: American Journal of Science, v. 290-A, p. 295–332.

Christie-Blick, N., Dyson, I. A., and Von Der Borch, C. C., 1995, Sequence stratigraphy and the interpretation of Neoproterozoic Earth history: Precambrian Research, v. 73, n. 1–4, p. 3–26, http://dx.doi.org/10.1016/0301-9268(94)00096-A

Condon, D., Zhu, M., Bowring, S., Wang, W., Yang, A., and Jin, Y., 2005, U-Pb ages from the Neoproterozoic Doushantuo Formation, China: Science, v. 308, n. 5718, p. 95–98, http://dx.doi.org/10.1126/science.1107765

Corsetti, F. A., Awramik, S. M., and Pierce, D., 2003, A complex microbiota from snowall Earth times: Microfossils from the Neoproterozoic Kingston Peak Formation, Death Valley, USA: Proceedings of the National Academy of Sciences of the United States of America, v. 100, n. 8, p. 4399–4404, http://dx.doi.org/10.1073/pnas.0730560100

DeCelles, P. G., Quade, J., Kapp, P., Fan, M., Dettman, D. L., and Ding, L., 2007, High and dry in central Tibet during the Late Oligocene: Earth and Planetary Science Letters, v. 253, n. 3–4, p. 389–401, http://dx.doi.org/10.1016/j.epsl.2006.11.001

Deevey, E. S., Jr., Nakai, N., and Stuiver, M., 1963, Fractionation of sulfur and carbon isotopes in a meromictic lake: Science, v. 139, n. 3553, p. 407–407, http://dx.doi.org/10.1126/science.139.3553.407

Derry, L. A., 2010, A burial diagenesis origin for the Ediacaran Shuram-Wonoka carbon isotope anomaly:

Earth and Planetary Science Letters, v. 294, n. 1–2, p. 152–162, http://dx.doi.org/10.1016/j.epsl.2010.03.022
DiBona, P. A., and von der Borch, C. C., 1993, Sedimentary geology and evolution of an outcropping shelf-margin delta, Late Proterozoic Wonoka Formation, South Australia: AAPG Bulletin, v. 77, n. 6, p. 963–979.
Dyson, I., 1992a, Stratigraphic nomenclature and sequence stratigraphy of the lower Wilpena Group, Adelaide Geosyncline: the Sandison Subgroup: Geological Survey of South Australia Quarterly Geology Notes, v. 122, p. 2–13.
Eberli, G. P., Anselmetti, F. S., Kroon, D., Sato, T., and Wright, J. D., 2002, The chronostratigraphic significance of seismic reflections along the Bahamas Transect: Marine Geology, v. 185, n. 1–2, p. 1–17, http://dx.doi.org/10.1016/S0025-3227(01)00287-0
Eickhoff, K. H., Vonderborch, C. C., and Grady, A. E., 1988, Proterozoic canyons of the Flinders Ranges (South-Australia): submarine canyons or drowned river valleys?: Sedimentary Geology, v. 58, n. 2–4, p. 217–235, http://dx.doi.org/10.1016/0037-0738(88)90070-X
Fike, D. A., Grotzinger, J. P., Pratt, L. M., and Summon, R. E., 2006, Oxidation of the Ediacaran ocean: Nature, v. 444, p. 744–747, http://dx.doi.org/10.1038/nature05345
Flügel, E., 2004, Microfacies in carbonate rocks: analysis, interpretation and application: Berlin-Heidelberger, Springer-Verlag, 976 p.
Fry, B., Jannasch, H. W., Molyneaux, S. J., Wirsen, C. O., Muramoto, J. A., and King, S., 1991, Stable isotope studies of the carbon, nitrogen and sulfur cycles in the Black Sea and the Cariaco Trench: Deep Sea Research Part A. Oceanographic Research Papers, v. 38, p. S1003–S1019.
Furukawa, Y., Lavoie, D., and Stephens, K., 1997, Effect of biogeochemical diagenesis on sediment fabric in shallow marine carbonate sediments near the Dry Tortugas, Florida: Geo-Marine Letters, v. 17, n. 4, p. 283–290, http://dx.doi.org/10.1007/s003670050039
Giddings, J. A., Wallace, M. W., Haines, P. W., and Mornane, K., 2010, Submarine origin for the Neoproterozoic Wonoka canyons, South Australia: Sedimentary Geology, v. 223, n. 1–2, p. 35–50, http://dx.doi.org/10.1016/j.sedgeo.2009.10.001
Gostin, V. A., Haines, P. W., Jenkins, R. J. F., Compston, W., and Williams, I. S., 1986, Impact ejecta horizon within late Precambrian shales, Adelaide Geosyncline, South Australia: Science, v. 233, n. 4760, p. 198–200, http://dx.doi.org/10.1126/science.233.4760.198
Grotzinger, J. P., and James, N. P., 2000, Precambrian carbonates: Evolution of understanding, *in* Grotzinger, J. P., and James, N. P., editors, Carbonate Sedimentation and Diagenesis in the Evolving Precambrian World: Society for Sedimentary Geology Special Publication 67, p. 3–20, http://dx.doi.org/10.2110/pec.00.67.0003
Grotzinger, J. P., Fike, D. A., and Fischer, W. W., 2011, Enigmatic origin of the largest-known carbon isotope excursion in Earth"s history: Nature Geoscience, v. 4, p. 285–292, http://dx.doi.org/10.1038/ngeo1138
Haggerty, J. A., 1991, Evidence from fluid seeps atop serpentine seamounts in the Mariana Forearc: Clues for emplacement of the seamounts and their relationship to forearc tectonics: Marine Geology, v. 102, n. 1–4, p. 293–309, http://dx.doi.org/10.1016/0025-3227(91)90013-T
Haines, P., ms, 1987, Carbonate shelf and basin sedimentation, late Proterozoic Wonoka Formation, South Australia: Adelaide, Australia, University of Australia, Ph. D. thesis, 152 p.
Haines, P. W., 1988, Storm-dominated mixed carbonate/siliciclastic shelf sequence displaying cycles of hummocky cross-stratification, late Proterozoic Wonoka Formation, South Australia: Sedimentary Geology, v. 58, n. 2–4, p. 237–254, http://dx.doi.org/10.1016/0037-0738(88)90071-1
——— 1990, A late Proterozoic storm-dominated carbonate shelf sequence: The Wonoka Formation in central and southern Flinders Ranges, South Australia, *in* Jago, J. B., and Moore, R. S., editors, The evolution of a Late Precambrian-Early Palaeozoic rift: Adelaide Geosyncline: Geological Society of Australia Special Publication, v. 16, p. 177–198.
Halverson, G., Hoffman, P., Maloof, A., Schrag, D., Rice, A. H. N., Bowring, S., and Dudas, F., 2005, Toward a Neoproterozoic composite carbon-isotope record: Geological Society of America Bulletin, v. 117, p. 1181–1207.
Halverson, G. P., Maloof, A. C., Schrag, D. P., Dudas, F. O., and Hurtgen, M., 2007, Stratigraphy and geochemistry of a *ca.* 800 Ma negative carbon isotope interval in northeastern Svalbard: Chemical Geology, v. 237, n. 1–2, p. 5–27, http://dx.doi.org/10.1016/j.chemgeo.2006.06.013
Higgins, J. A., and Schrag, D. P., 2006, Beyond methane: Towards a theory for the Paleocene- Eocene Thermal Maximum: Earth and Planetary Science Letters, v. 245, p. 523–537, http://dx.doi.org/10.1016/j.epsl.2006.03.009
Higgins, J. A., Fischer, W. W., and Schrag, D. P., 2009, Oxygenation of the ocean and sediments: Consequences for the seafloor carbonate factory: Earth and Planetary Science Letters, v. 284, n. 1–2, p. 25–33, http://dx.doi.org/10.1016/j.epsl.2009.03.039
Hill, A. C., and Walter, M. R., 2000, Mid-Neoproterozoic (~830-750 Ma) isotope stratigraphy of Australia and global correlation: Precambrian Research, v. 100, n. 1–3, p. 181–211, http://dx.doi.org/10.1016/S0301-9268(99)00074-1
Hoffman, P. F., Kaufman, A. J., Halverson, G. P., and Schrag, D. P., 1998, A Neoproterozoic snowball Earth: Science, v. 281, n. 5381, p. 1342–1346, http://dx.doi.org/10.1126/science.281.5381.1342
Hoffmann, K.-H., Condon, D. J., Bowring, S. A., and Crowley, J. L., 2004, U-Pb zircon date from the Neoproterozoic Ghaub Formation, Namibia: Constraints on Marinoan glaciation: Geology, v. 32, n. 9, p. 817–820, http://dx.doi.org/10.1130/G20519.1
Husson, J. M., Maloof, A. C., and Schoene, B., 2012, A syn-depositional age for Earth's deepest $\delta^{13}C$ excursion required by isotope conglomerate tests: Terra Nova, v. 24, n. 4, p. 318–325, http://dx.doi.org/10.1111/j.1365-3121.2012.01067.x

Jacobsen, S. B., and Kaufman, A. J., 1999, The Sr, C, and O isotopic evolution of Neoproterozoic seawater: Chemical Geology, v. 161, n. 1–3, p. 37–57, http://dx.doi.org/10.1016/S0009-2541(99)00080-7

Johnston, D. T., Poulton, S. W., Goldberg, T., Sergeev, V. N., Podkovyrov, V., Vorob'eva, N. G., Bekker, A., and Knoll, A. H., 2012, Late Ediacaran redox stability and metazoan evolution: Earth and Planetary Science Letters, v. 335–336, p. 25–35, http://dx.doi.org/10.1016/j.epsl.2012.05.010

Kaufman, A. J., Corsetti, F. A., and Varni, M. A., 2007, The effect of rising atmospheric oxygen on carbon and sulfur isotope anomalies in the Neoproterozoic Johnnie Formation, Death Valley, USA: Chemical Geology, v. 237, n. 1–2, p. 47–63, http://dx.doi.org/10.1016/j.chemgeo.2006.06.023

Kennedy, M. J., 1996, Stratigraphy, sedimentology, and isotopic geochemistry of Australian Neoproterozoic postglacial cap dolostones: Deglaciation, $\delta^{13}C$ excursions, and carbonate precipitation: Journal of Sedimentary Research, v. 66, n. 6, p. 1050–1064, http://dx.doi.org/10.2110/jsr.66.1050

Kennett, J. P., and Stott, L. D., 1991, Abrupt deep-sea warming, palaeoceanographic changes and benthic extinctions at the end of the Palaeocene: Nature, v. 353, p. 225–229, http://dx.doi.org/10.1038/353225a0

Knauth, L. P., and Kennedy, M. J., 2009, The late Precambrian greening of the Earth: Nature, v. 460, p. 728–732, http://dx.doi.org/10.1038/nature08213

Knoll, A. H. and Walter, M. R., 1992, Latest Proterozoic stratigraphy and Earth history: Nature, v. 356, p. 673–678, http://dx.doi.org/10.1038/356673a0

Knoll, A. H., Walter, M. R., Narbonne, G. M., and Christie-Blick, N., 2006, The Ediacaran Period: a new addition to the geologic time scale: Lethaia, v. 39, p. 13–30, http://dx.doi.org/10.1080/00241160500409223

Kretz, R., 1982, A model for the distribution of trace elements between calcite and dolomite: Geochimica et Cosmochimica Acta, v. 46, n. 10, p. 1979–1981, http://dx.doi.org/10.1016/0016-7037(82)90137-5

Kroopnick, P., 1985, The distribution of ^{13}C of ΣCO_2 in the world oceans: Deep Sea Research Part A. Oceanographic Research Papers, v. 32, n. 1, p. 57–84, http://dx.doi.org/10.1016/0198-0149(85)90017-2

Lazar, B., and Erez, J., 1992, Carbon geochemistry of marine-derived brines: I. ^{13}C depletions due to intense photosynthesis: Geochimica et Cosmochimica Acta, v. 56, n. 1, p. 335–345, http://dx.doi.org/10.1016/0016-7037(92)90137-8

Le Guerroué, E., Allen, P. A., and Cozzi, A., 2006a, Chemostratigraphic and sedimentological framework of the largest negative carbon isotopic excursion in Earth history: The Neoproterozoic Shuram Formation (Nafun Group, Oman): Precambrain Research, v. 146, n. 1–2, p. 68–92, http://dx.doi.org/10.1016/j.precamres.2006.01.007

——— 2006b, Parasequence development in the Ediacaran Shuram Formation (Nafun Group, Oman): high resolution stratigraphic test for primary origin of negative carbon isotopic ratios: Basin Research, v. 18, n. 2, p. 205–219, http://dx.doi.org/10.1111/j.1365-2117. 2006.00292.x

Le Guerroué, E., Allen, P., Cozzi, A., Etienne, J., and Fanning, M., 2006c, 50 Myr recovery from the largest negative $\delta^{13}C$ excursion in the Ediacaran ocean: Terra Nova, v. 18, n. 2, p. 147–153, http://dx.doi.org/10.1111/j.1365-3121.2006.00674.x

Lee, C., Fike, D. A., Love, G. D., Sessions, A. L., Grotzinger, J. P., Summons, R. E., and Fischer, W. W., 2013, Carbon isotopes and lipid biomarkers from organic-rich facies of the Shuram Formation, Sultanate of Oman: Geobiology, v. 11, n. 5, p. 406–419, http://dx.doi.org/10.1111/gbi.12045

Lorens, R. B., 1981, Sr, Cd, Mn and Co distribution coefficients in calcite as a function of calcite precipitation rate: Geochimica et Cosmochimica Acta, v. 45, n. 4, p. 553–561, http://dx.doi.org/10.1016/0016-7037(81)90188-5

Love, G. D., Grosjean, E., Stalvies, C., Fike, D. A., Grotzinger, J. P., Bradley, A. S., Kelly, A. E., Bhatia, M., Meredith, W., Snape, C. E., Bowring, S. A., Condon, D. J., and Summons, R. E., 2009, Fossil steroids record the appearance of Demospongiae during the Cryogenian: Nature, v. 457, p. 718–721, http://dx.doi.org/10.1038/nature07673

Lowenstein, T. K., Timofeeff, M. N., Brennan, S. T., Hardie, L. A., and Demicco, R. V., 2001, Oscillations in phanerozoic seawater chemistry: Evidence from fluid inclusions: Science, v. 294, n. 5544, p. 1086–1088, http://dx.doi.org/10.1126/science.1064280

Loyd, S. J., Marenco, P. J., Hagadorn, J. W., Lyons, T. W., Kaufman, A. J., Sour-Tovar, F., and Corsetti, F. A., 2012, Sustained low marine sulfate concentrations from the Neoproterozoic to the Cambrian: Insights from carbonates of northwestern Mexico and eastern California: Earth and Planetary Science Letters, v. 339, p. 79–94, http://dx.doi.org/10.1016/j.epsl.2012.05.032

Macdonald, F. A., Strauss, J. V., Sperling, E. A., Halverson, G. P., Narbonne, G. M., Johnston, D. T., Kunzmann, M., Schrag, D. P., and Higgins, J. A., 2013, The stratigraphic relationship between the Shuram carbon isotope excursion, the oxygenation of Neoproterozoic oceans, and the first appearance of the Ediacara biota and bilaterian trace fossils in northwestern Canada: Chemical Geology, v. 362, p. 250–272, http://dx.doi.org/10.1016/j.chemgeo.2013.05.032

Macintyre, I. G. and Reid, R. P., 1995, Crystal alteration in a living calcareous alga (Halimeda); implications for studies in skeletal diagenesis: Journal of Sedimentary Research, v. 65, n. 1a, p. 143–153, http://dx.doi.org/10.1306/D4268054-2B26-11D7-8648000102C1865D

Maloof, A. C., Halverson, G. P., Kirschvink, J. L., Schrag, D. P.,Weiss, B. P., and Hoffman, P. F., 2006, Combined paleomagnetic, isotopic and stratigraphic evidence for true polar wander from the Neoproterozoic Akademikerbreen Group, Svalbard, Norway: GSA Bulletin, v. 118, n. 9–10, p. 1099–1124, http://dx.doi.org/10.1130/B25892.1

Maloof, A. C., Rose, C. V., Beach, R., Samuels, B. M., Calmet, C. C., Erwin, D. H., Poirier, G. R., Yao, N., and Simons, F. J., 2010, Possible animal-body fossils in pre-Marinoan limestones from South Australia: Nature Geoscience, v. 3, p. 653–659, http://dx.doi.org/10.1038/ngeo934

McFadden, K. A., Huang, J., Chu, X., Jiang, G., Kaufman, A. J., Zhou, C., Yuan, X., and Xiao, S., 2008, Pulsed oxidation and biological evolution in the Ediacaran Doushantuo Formation: Proceedings of the

National Academy of Sciences of the United States of America, v. 105, n. 9, p. 3197–3202, http://dx.doi.org/10.1073/pnas.0708336105
Melezhik, V. A., Roberts, D., Fallick, A. E., and Gorokhov, I. M., 2008, The Shuram-Wonoka event recorded in a high-grade metamorphic terrane: insight from the Scandinavian Caledonides: Geological Magazine, v. 145, n. 2, p. 161–172, http://dx.doi.org/10.1017/S0016756807004189
Melezhik, V. A., Pokrovsky, B. G., Fallick, A. E., Kuznetsov, A. B., and Bujakaite, M. I., 2009, Constraints on $^{87}Sr/^{86}Sr$ of late Ediacaran seawater: insight from Siberian high-Sr limestones: Journal of the Geological Society, London, v. 166, n. 1, p. 183–191, http://dx.doi.org/10.1144/0016-76492007-171
Melim, L. A., Swart, P. K., and Maliva, R. G., 2001, Meteoric and marine-burial diagenesis in the subsurface of Great Bahama Bank: Special Publication-SEPM, v. 70, p. 137–162.
Neuweiler, F., Turner, E. C., and Burdige, D. J., 2009, Early Neoproterozoic origin of the metazoan clade recorded in carbonate rock texture: Geology, v. 37, n. 5, p. 475–478, http://dx.doi.org/10.1130/G25621A.1
Oehlert, A. M., Lamb-Wozniak, K. A., Devlin, Q. B., Mackenzie, G. J., Reijmer, J. J. G., and Swart, P. K., 2012, The stable carbon isotopic composition of organic material in platform derived sediments: implications for reconstructing the global carbon cycle: Sedimentology, v. 59, n. 1, p. 319–335, http://dx.doi.org/10.1111/j.1365-3091.2011.01273.x
Paul, D., Skrzypek, G., and Fórizs, I., 2007, Normalization of measured stable isotopic compositions to isotope reference scales–a review: Rapid Communications in Mass Spectrometry, v. 21, n. 18, p. 3006–3014, http://dx.doi.org/10.1002/rcm.3185
Peters, S. E., 2006, Macrostratigraphy of North America: The Journal of Geology, v. 114, n. 4, p. 391–412, http://dx.doi.org/10.1086/504176
Pingitore, N. E., Jr., 1978, The behavior of Zn^{2+} and Mn^{2+} during carbonate diagenesis: theory and applications: Journal of Sedimentary Research, v. 48, n. 3, p. 799–814, http://dx.doi.org/10.1306/212F756D-2B24-11D7-8648000102C1865D
Plummer, P., 1979, Note on the palaeoenvironmental significance of the Nuccaleena Formation (upper Precambrian, central Flinders Ranges, South Australia: Journal of the Geological Society of Australia, v. 25, n. 7–8, p. 395–402, http://dx.doi.org/10.1080/00167617808729049
Pokrovskii, B. G., Melezhik, V. A., and Bujakaite, M. I., 2006, Carbon, oxygen, strontium, and sulfur isotopic compositions in late Precambrian rocks of the Patom Complex, central Siberia: Communication 1. Results, isotope stratigraphy, and dating problems: Lithology and Mineral Resources, v. 41, n. 5, p. 450–474, http://dx.doi.org/10.1134/S0024490206050063
Pratson, L. F., and Coakley, B. J., 1996, A model for the headward erosion of submarine canyons induced by downslope-eroding sediment flows: Geological Society of America Bulletin, v. 108, n. 2, p. 225–234, http://dx.doi.org/10.1130/0016-7606(1996)108<0225:AMFTHE>2.3.CO;2
Prave, A. R., Fallick, A. E., Thomas, C. W., and Graham, C. M., 2009, A composite C-isotope profile for the Neoproterozoic Dalradian Supergroup of Scotland and Ireland: Journal of the Geological Society, London, v. 166, n. 5, p. 845–857, http://dx.doi.org/10.1144/0016-76492008-131
Preiss, W., 1987, Stragraphic nomenclature and classification, *in* Preiss, W., editor, The Adelaide Geosyncline of South Australia, Late Proterozoic stratigraphy, sedimentation, palaeontology and tectonics: Geological Survey of South Australia, Bulletin v. 53, p. 29–34.
Preiss, W. V., 2000, The Adelaide Geosyncline of South Australia and its significance in Neoproterozoic continental reconstruction: Precambrian Research, v. 100, n. 1–3, p. 21–63, http://dx.doi.org/10.1016/S0301-9268(99)00068-6
Pruss, S. B., Corsetti, F. A., and Fischer, W. W., 2008, Seafloor-precipitated carbonate fans in the Neoproterozoic Rainstorm Member, Johnnie Formation, Death Valley Region, USA: Sedimentary Geology, v. 207, n. 1–4, p. 34–40, http://dx.doi.org/10.1016/j.sedgeo.2008.03.005
Raymond, O. L., Liu, S., Gallagher, R., Highet, L., and Zhang, W., 2012, Surface geology of Australia, 1:1 000 000 scale, 2012 edition [digital dataset]: Canberra, Geoscience Australia, Commonwealth of Australia, Technical report, Geoscience Australia.
Reid, R. P., and Macintyre, I. G., 1998, Carbonate recrystallization in shallow marine environments: a widespread diagenetic process forming micritized grains: Journal of Sedimentary Research, v. 68, n. 5, p. 928–946, http://dx.doi.org/10.2110/jsr.68.928
Retallack, G. J., 2013, Ediacaran life on land: Nature, v. 493, p. 89–92, http://dx.doi.org/10.1038/nature11777
Rose, C. V., and Maloof, A. C., 2010, Testing models for post-glacial "cap dolostone" deposition: Nuccaleena Formation, South Australia: Earth and Planetary Science Letters, v. 296, n. 3–4, p. 165–180, http://dx.doi.org/10.1016/j.epsl.2010.03.031
Rose, C. V., Maloof, A. C., Schoene, B., Ewing, R. C., Linnemann, U., Hofmann, M., and Cottle, J. M., 2013, The end-Cryogenian glaciation of South Australia: Geoscience Canada, v. 40, n. 4, p. 256–293, http://dx.doi.org/10.12789/geocanj.2013.40.019
Rothman, D. H., Hayes, J. M., and Summons, R. E., 2003, Dynamics of the Neoproterozoic carbon cycle: Proceedings of the National Academy of Sciences of the United States of America, v. 100, n. 4, p. 8124–8129, http://dx.doi.org/10.1073/pnas.0832439100
Sadler, P. M., 1981, Sediment accumulation rates and the completeness of stratigraphic sections: The Journal of Geology, v. 89, n. 5, p. 569–584, http://dx.doi.org/10.1086/628623
Saylor, B. Z., Kaufman, A. J., Grotzinger, J. P., and Urban, F., 1998, A composite reference section for terminal Proterozoic strata of southern Namibia: Journal of Sedimentary Research, v. 68, n. 6, p. 1223–1235, http://dx.doi.org/10.2110/jsr.68.1223
Schrag, D. P., Higgins, J. A., Macdonald, F. A., and Johnston, D. T., 2013, Authigenic carbonate and the history of the global carbon cycle: Science, v. 339, n. 6119, p. 540–543, http://dx.doi.org/10.1126/science.1229578

Scott, C., Lyons, T. W., Bekker, A., Shen, Y., Poulton, S. W., Chu, X., and Anbar, A. D., 2008, Tracing the stepwise oxygenation of the Proterozoic ocean: Nature, v. 452, p. 456–459, http://dx.doi.org/10.1038/nature06811

Sperling, E. A., Robinson, J. M., Pisani, D., and Peterson, K. J., 2010, Where's the glass? Biomarkers, molecular clocks, and microRNAs suggest a 200-Myr missing Precambrian fossil record of siliceous sponge spicules: Geobiology, v. 8, n. 1, p. 24–36, http://dx.doi.org/10.1111/j.1472-4669.2009.00225.x

Swanson-Hysell, N. L., Maloof, A. C., Kirschvink, J. L., Evans, D. A. D., Halverson, G. P., and Hurtgen, M. T., 2012, Constraints on Neoproterozoic paleogeography and Paleozoic orogenesis from paleomagnetic records of the Bitter Springs Formation, Amadeus Basin, central Australia: American Journal of Science, v. 312, n. 8, p. 817–884, http://dx.doi.org/10.2475/08.2012.01

Swart, P. K., 2008, Global synchronous changes in the carbon isotopic composition of carbonate sediments unrelated to changes in the global carbon cycle: Proceedings of the National Academy of Sciences of the United States of America, v. 105, n. 37, p. 13,741–13,745, http://dx.doi.org/10.1073/pnas.0802841105

Swart, P. K., and Eberli, G., 2005, The nature of the $\delta^{13}C$ of periplatform sediments: Implications for stratigraphy and the global carbon cycle: Sedimentary Geology, v. 175, n. 1–4, p. 115–129, http://dx.doi.org/10.1016/j.sedgeo.2004.12.029

Swart, P. K., and Kennedy, M. J., 2012, Does the global stratigraphic reproducibility of $\delta^{13}C$ in Neoproterozoic carbonates require a marine origin? A Pliocene–Pleistocene comparison: Geology, v. 40, n. 1, p. 87–90, http://dx.doi.org/10.1130/G32538.1

Tessier, A., Campbell, P. G. C., and Bisson, M., 1979, Sequential extraction procedure for the speciation of particulate trace metals: Analytical Chemistry, v. 51, n. 7, p. 844–851, http://dx.doi.org/10.1021/ac50043a017

Thomson, B., Coats, R., Mirams, R., Forbes, B., Dalgarno, C., and Johnson, J., 1964, Precambrian rock groups in the Adelaide Geosyncline: new subdivision: Quarterly Journal of the Geological Survey of South Australia, v. 9, p. 1–19.

Verdel, C., Wernicke, B. P., and Bowring, S. A., 2011, The Shuram and subsequent Ediacaran carbon isotope excursions from southwest Laurentia, and implications for environmental stability during the metazoan radiation: Geological Society of America Bulletin, v. 123, n. 7–8, p. 1539, http://dx.doi.org/10.1130/B30369.1

von der Borch, C. C., Grady, A. E., Eickhoff, K. H., DiBona, P., and Christie-Blick, N., 1989, Late Proterozoic Patsy Springs Canyon, Adelaide Geosyncline: submarine or subaerial origin?: Sedimentology, v. 36, n. 5, p. 777–792, http://dx.doi.org/10.1111/j.1365-3091.1989.tb01746.x

Wallace, M. W., and Woon, E., 2008, Giant Cryogenian reefs as windows into pre-Ediacaran life, *in* Selwyn Symposium: Neoproterozoic climates and the origin of Early Life: Geological Society of Australia Victoria Division, v. 91, p. 17–21.

Walter, L. M., and Morse, J. W., 1984, Reactive surface area of skeletal carbonates during dissolution; effect of grain size: Journal of Sedimentary Research, v. 54, n. 4, p. 1081–1090, http://dx.doi.org/10.1306/212F8562-2B24-11D7-8648000102C1865D

Walter, L. M., Ku, T. C. W., Muehlenbachs, K., Patterson, W. P., and Bonnell, L., 2007, Controls on the $\delta^{13}C$ of dissolved inorganic carbon in marine pore waters: An integrated case study of isotope exchange during syndepositional recrystallization of biogenic carbonate sediments (South Florida Platform, USA): Deep Sea Research Part II: Topical Studies in Oceanography, v. 54, n. 11–13, p. 1163–1200, http://dx.doi.org/10.1016/j.dsr2.2007.04.014

Williams, G., 1977, Late Precambrian dolomites, Vendian glaciation, and synchroneity of Vendian glaciations: A discussion: The Journal of Geology, v. 85, n. 2, p. 250–251, http://dx.doi.org/10.1086/628291

Williams, G. E., 1979, Sedimentology, stable-isotope geochemistry and palaeoenvironment of dolostones capping late Precambrian glacial sequences in Australia: Journal of the Geological Society of Australia, v. 26, n. 7–8, p. 377–386, http://dx.doi.org/10.1080/00167617908729104

Workman, R. K., Grotzinger, J. P., and Hart, S. R., 2002, Constraints on Neoproterozoic ocean chemistry from $\delta^{13}C$ and $\delta^{11}B$ analyses of carbonates from the Witvlei and Nama Groups, Namibia: Geochimica et Cosmochimica Acta, v. 66, n. 15A, p. A847.

Xiao, S., and Laflamme, M., 2009, On the eve of animal radiation: phylogeny, ecology and evolution of the Ediacara biota: Trends in Ecology & Evolution, v. 24, n. 1, p. 31–40, http://dx.doi.org/10.1016/j.tree.2008.07.015

Xiao, S., Droser, M., Gehling, J. G., Hughes, I. V., Wan, B., Chen, Z., and Yuan, X., 2013, Affirming life aquatic for the Ediacara biota in China and Australia: Geology, v. 41, n. 10, p. 1095–1098, http://dx.doi.org/10.1130/G34691.1

Zachos, J. C., Röhl, U., Schellenberg, S. A., Sluijs, A., Hodell, D. A., Kelly, D. C., Thomas, E., Nicolo, M., Raffi, I., Lourens, L. J., McCarren, H., and, Kroon, D., 2005, Rapid acidification of the ocean during the Paleocene-Eocene thermal maximum: Science, v. 308, n. 5728, p. 1611–1615, http://dx.doi.org/10.1126/science.1109004